2017-07

Semi-quantitative reconstruction of early to late Holocene spring and summer sea ice conditions in the northern Barents Sea

Berben, SMP

10.1002/jqs.2953
Journal of Quaternary Science
Wiley

Semi-quantitative reconstruction of early to late Holocene spring and summer sea ice conditions in the northern Barents Sea

Sarah M.P. Berben[a,1], Katrine Husum[b], Alba Navarro-Rodriguez[c], Simon T. Belt[c], Steffen Aagaard-Sørensen[a]

[a] *Department of Geology, UiT – The Arctic University of Norway, N-9037 Tromsø, Norway*

[b] *Norwegian Polar Institute, Fram Centre, N-9296 Tromsø, Norway*

[c] *Biogeochemistry Research Centre, School of Geography, Earth and Environmental Sciences, University of Plymouth, Drake Circus, Plymouth PL4 8AA, UK*

[1]Corresponding author.

E-mail address:sarah.berben@uib.no

Current address: Department of Earth Science, University of Bergen and the Bjerknes Centre for Climate Research, N-5007 Bergen, Norway

Abstract

Semi-quantitative estimates of early to late Holocene spring sea ice concentration (SpSIC) and occurrence of summer sea ice for the northern Barents Sea have been obtained by analysing the biomarkers IP_{25}, brassicasterol and a tri-unsaturated highly branched isoprenoid lipid in a Holocene marine sediment core. Sub-surface water mass variations were derived from planktic foraminiferal assemblages and stable isotopes ($\delta^{18}O$, $\delta^{13}C$). The record indicates paleoceanographic changes over three intervals. During Period I (ca. 9500–5900 cal a BP), the study location experienced the lowest recorded SpSIC (ca. 25%) with short spring seasons and long productive summers, resulting partly from increased Atlantic Water inflow that caused a stronger ocean-atmosphere heat exchange. Throughout Period II (ca. 5900–2700 cal a BP), the winter sea ice margin migrated southwards and an overall cooling trend resulted in higher SpSIC (ca. 60%) and increased delivery of cold Arctic Water. During Period III (ca. 2700 cal a BP–present), SpSIC increased further (ca. 75%) and some sea ice remained during summer months. A sub-surface warming likely indicates a decoupling of heat exchange between the ocean and the atmosphere. Longer springs and shorter summers were accompanied by the most southerly location of the winter sea ice margin.

Keywords

Sea ice, biomarker, proxy data, Holocene, Arctic

Introduction

The Barents Sea is a relatively small and shallow sea, yet it plays a crucial role in the Arctic climate system, in part, because of significant heat exchange between the ocean and the atmosphere (Serreze *et al.,* 2007). Oceanic heat is brought into the Barents Sea via the inflow of warm Atlantic water and, due to shallow depths, heat loss to the atmosphere is very efficient. Further, it has been suggested that ocean advection strongly influences sea ice conditions in the Barents Sea, so the region is central to understanding ocean-sea ice-atmosphere interactions (Vinje, 2001).

Recently, many Arctic regions have experienced an abrupt decline in sea ice conditions, with the northern Barents Sea and the Chukchi Sea identified as the most affected areas during the last three to four decades (Screen and Simmonds, 2010; Stroeve *et al.,* 2007, 2012). Present day sea ice variations within the Barents Sea have been attributed to different processes (e.g. atmospheric circulation variability, local wind patterns, ice import from the Arctic interior to the Barents Sea), although the role of oceanic heat advection is often emphasized as one of the most important factors (e.g. Årthun *et al*., 2012; Ivanov *et al*., 2012; Smedsrud *et al*., 2013). For example, Årthun *et al*. (2012) argued that recent increases in Atlantic Water inflow to the Barents Sea has contributed to a further decline in sea ice conditions in the Barents Sea. Similarly, the northerly inflow of Pacific Water has been suggested as a contributing factor to reduced sea ice conditions in the Chukchi Sea in recent times (e.g. Shimada *et al.,* 2006; Woodgate *et al.,* 2010) and during the Holocene (Stein *et al.,* 2016a).

Since the impacts of Arctic amplification and the associated sea ice decline (Serreze and Francis, 2006; Screen and Simmonds, 2010) reach far beyond the Arctic region (Yang and Christensen, 2012), it is clearly necessary to better understand the interaction between sea ice production and water mass conditions, together with any natural variability that occurs between them over longer time frames. Instrumental and observational records of past climate variations in the Barents Sea reach back only ca. 100–150 years (Divine and Dick, 2006; Smedsrud *et al*., 2013), so longer-term records of sea ice and water mass conditions need to be derived from proxy climate indicators archived in marine sediment cores. Such records from the northern Barents Sea (e.g. Duplessy *et al*., 2001; Lubinski *et al*., 2001; Risebrobakken *et al*., 2011; Klitgaard Kristensen *et al*., 2013), the western Barents Sea (Berben *et al*., 2014) and the Svalbard margin (e.g. Slubowska *et al*., 2005; Rasmussen *et al*.,

2007; Spielhagen *et al*., 2011; Müller *et al*., 2012; Werner *et al*., 2013) have demonstrated various fluctuations of both the influence of Atlantic Water inflow to the Barents Sea and sea ice conditions throughout the Holocene. The observed Holocene changes in the region have mainly been attributed to insolation changes and further factors such as land-cover feedbacks and coupled atmospheric-oceanic dynamics, in particular the northward penetration of relatively warm Atlantic Water (Berger, 1978; Koç *et al.,* 1993; Kaufman *et al.,* 2004). Additionally, insolation forcing has also been attributed to the long-term sea ice variability (Müller *et al.,* 2012; Cabedo-Sanz *et al.,* 2016b). However, few of these reconstructions have employed a specific proxy for sea ice or have provided detailed descriptions of sea ice conditions, including semi-quantitative estimates of spring sea ice concentration (SpSIC) or summer sea ice occurrence.

In this study, the biomarkers IP_{25}, brassicasterol and a tri-unsaturated highly branched isoprenoid (HBI) lipid (HBI III) have been analyzed in a marine sediment core from the Olga Basin in order to reconstruct a detailed record of sea ice conditions for the early to late Holocene in the northern Barents Sea (Fig. 1). The biomarker concentration data were presented previously by Belt *et al*. (2015), but were not discussed in detail. In the current study, therefore, we provide a more in-depth discussion of the individual and combined (i.e. PIP_{25}) biomarker data, including, for the first time, semi-quantitative estimates of SpSIC based on the recent calibration study by Smik *et al*. (2016). In addition, and similar to Werner *et al.* (2013, 2014), planktic foraminiferal fauna assemblages and stable carbon and oxygen isotopes ($\delta^{18}O$, $\delta^{13}C$) have also been measured to obtain a combined multiproxy record of sea ice conditions and sub-surface water masses, thus demonstrating the interaction of sea ice and inflow of Atlantic Water. The study site is located between the Atlantic Water characterized southern Barents Sea and the central Arctic Ocean and is, therefore, influenced by Atlantic derived water masses (Abrahamsen *et al*., 2006) but also experiences seasonal sea ice conditions (Fig. 1). As such, it represents a key location for reconstructing Holocene changes in sea ice conditions and Atlantic Water inflow. Using our Holocene proxy data, we also propose different oceanographic scenarios that emphasize the changing interactions between sea ice conditions and near-surface waters and these are discussed further by comparing the proxy data with outcomes from previous studies from the region.

Sea ice biomarker background information

Following the initial discovery of the Arctic sea ice proxy IP_{25} (Belt *et al*., 2007), analysis of this biomarker has subsequently led to sea ice reconstructions for various sub-Arctic and Arctic regions: the central Arctic Ocean (Xiao *et al.,* 2015a, 2015b), the Labrador Sea (Weckström *et al.,* 2013), the Canadian Arctic (Vare *et al*., 2009), the Bering Sea/North Pacific (Méheust *et al.,* 2013, 2015), the Chukchi Sea (Polyak *et al.,* 2016; Stein *et al.,* 2016a), the East Siberian Sea (Stein *et al.,* 2016a), the Laptev Sea (Fahl and Stein 2012; Xiao *et al.,* 2013), the Barents Sea (Vare *et al.,* 2010; Berben *et al*., 2014), the Fram Strait (Müller *et al*., 2009, 2012; Cabedo-Sanz *et al*., 2013, 2016a; Knies *et al*., 2014; Müller and Stein, 2014) and the Greenland/Norwegian Seas (Massé *et al.,* 2008; Cabedo-Sanz *et al.,* 2016b). Furthermore, IP_{25} appears stable within Arctic sediments to permit sea ice reconstructions over even longer timescales (e.g. going back into the Pliocene (Knies *et al.,* 2014) and the Miocene (Stein *et al.,* 2016b). IP_{25} is biosynthesized by certain Arctic sea ice diatoms and is thus usually found in areas with seasonal sea ice conditions (e.g. Belt *et al*., 2007; Brown *et al*., 2011, 2014; Belt and Müller, 2013). In order to provide complementary information regarding open water conditions, Müller *et al*. (2009) proposed the additional measurement of phytoplankton biomarkers, such as brassicasterol. In addition, by combining IP_{25} and phytoplankton biomarker concentrations, in the form of the so-called PIP_{25} index, a method of elucidating semi-quantitative estimates of sea ice conditions has been proposed (Müller *et al*., 2011). However, application of the PIP_{25} method is not always straightforward because some phytoplankton markers such as brassicasterol may also have non-pelagic sources and their generally higher concentration compared to IP_{25} requires the use of a balance factor in the calculation of PIP_{25}, which can be problematic (for a detailed discussion, see Belt and Müller, 2013; Navarro-Rodriguez *et al*., 2013; Belt *et al*., 2015; Xiao *et al.,* 2015a; Smik *et al*., 2016). A recent study by Belt *et al*. (2015), however, demonstrated that a further phytoplankton-derived HBI biomarker, more specifically HBI III, was relatively abundant for locations within the marginal ice zone or close to the winter ice margin in the Barents Sea, thus representing an alternative indicator of open water conditions. In addition, since HBI III has a more constrained source (diatoms) and has sedimentary concentrations much closer to those of IP_{25}, some of the problems associated with using some other phytoplankton biomarkers can potentially be avoided. In a subsequent study, Smik *et al*. (2016) also demonstrated that PIP_{25} values based on IP_{25} and HBI III could provide realistic estimates of SpSIC for the Barents Sea, while a threshold value of 0.8 was suggested as providing evidence for the presence of summer sea ice (>5% summer sea ice concentration (SuSIC)).

Study area and oceanographic setting

The Barents Sea is an epicontinental shelf located between the Norwegian-Russian coast, Novaya Zemlya and the Svalbard and Franz Josef Land archipelagos (Fig. 1). The northern boundary of the Barents Sea is defined by the Nansen Basin continental slope (Jakobsson *et al*., 2004). The Barents Sea is characterized by several water masses and represents a major passage for Atlantic Water entering the Arctic Ocean (Carmack *et al*., 2006; Rudels *et al*., 2014).

The Norwegian Atlantic Current transports relatively warm and saline Atlantic Water towards the high latitude North Atlantic Ocean (Hopkins, 1991) (Fig. 1a). Before entering the Barents Sea, the Norwegian Atlantic Current splits into two different branches, the West Spitsbergen Current and the North Cape Current, respectively (Fig. 1a). Both of these currents transport the warm saline Atlantic Water into the Arctic Ocean (Rudels *et al*., 2014). Within the Barents Sea, Atlantic Water is entered from both the north and the southwest. The West Spitsbergen Current flows northwards along the western Barents Sea slope and splits into three branches in the Fram Strait; the Return Atlantic Current, the Yermak Branch and the Svalbard Branch (Fig. 1a) (e.g. Manley, 1995). The latter enters the Arctic Ocean north of Svalbard as a sub-surface current flowing eastward and beyond the Franz Victoria and St. Anna Troughs (Abrahamsen *et al*., 2006; Rudels *et al*., 2014). A sub-surface inflow of Atlantic Water derived from the Svalbard Branch enters the Barents Sea via the Northern Barents Sea Opening (Fig. 1a). Subsequently, Atlantic Water is advected south-westwards into the northern Barents Sea and has been observed year-round in the Olga Basin (Abrahamsen *et al*., 2006) where the studied sediment core is located. Although the major sub-surface water mass in the Olga Basin is Atlantic Water derived from the Svalbard Branch (Gammelsrød *et al.,* 2009; Klitgaard Kristensen *et al.,* 2013), the area is furthermore influenced by Atlantic Water that enters as a submerged flow from the south (e.g. Novitskiy, 1961; Loeng, 1991; Pfirman *et al*., 1994; Aksenov *et al*., 2010). The latter is brought to the area by the North Cape Current flowing northwards via the Barents Sea Opening into the southern Barents Sea, parallel to the coastal current system (Loeng, 1991; Loeng *et al*., 1993; Midttun, 1985; Rudels, 1987) (Fig. 1a). After mixing and heat loss, Atlantic Water exits the Barents Sea via the Barents Sea Exit and reaches the Arctic Ocean via the St. Anna Trough (e.g. Schauer *et al*., 2002; Rudels *et al*., 2014) (Fig. 1a).

In addition to relatively warm Atlantic Water, the Barents Sea is also influenced by Polar Water that is brought from the Arctic Ocean into the Barents Sea through the Franz Victoria and St. Anna Troughs, via the East Spitsbergen Current and the Bear Island Current, respectively (Hopkins, 1991) (Fig. 1a). Arctic Water is formed when relatively warm Atlantic Water converges and merges with cold, less saline and ice loaded Polar Water (Hopkins, 1991). Hence, surface water in the north-eastern Barents Sea is, in contrast to the Atlantic Water dominated south-western Barents Sea, dominated by Arctic Water characterized by reduced temperature and salinity, as well as seasonal sea ice conditions (Hopkins, 1991). A CTD profile taken at the core location illustrates the presence of Arctic Water at the surface, with Atlantic Water below ca. 150 m (Fig. 1c; Table S1).

The oceanic fronts dividing these different water masses are one of the main oceanographic features of the near-surface waters of the Barents Sea (Pfirman *et al*., 1994). Defined as a sharp climatic gradient in terms of temperature, salinity and sea ice conditions, the Polar and Arctic fronts are the respective boundaries between Polar/Arctic and Arctic/Atlantic waters. The positions of the Polar and Arctic fronts are closely related to the overall sea ice conditions and, in particular, align with the average summer and winter sea ice margins, respectively (Vinje, 1977). Although sea ice advection from the Arctic Ocean does occur, sea ice within the Barents Sea is mainly formed locally during autumn and winter (Loeng, 1991). The southward extent of the oceanic fronts, and hence the sea ice conditions in particular, are regulated by the inflow of Atlantic Water into the western Barents Sea, which controls the mainly ice-free Atlantic domain in the south-western Barents Sea (Årthun *et al*., 2012). In contrast, the north-eastern Barents Sea experiences large changes in seasonal sea ice conditions (Vinje, 2001; Sorteberg and Kvingedal, 2006) with maximum sea ice conditions during March/April and minimum occurring throughout August/September (Fig. 1b). Annual sea ice variability during recent decades might be explained by factors such as cyclone activity, which cause fluctuations in sea ice transport, to and from the Arctic Ocean into the north-eastern Barents Sea (Kwok *et al*., 2005; Sorteberg and Kvingedal, 2006; Ellingsen *et al*., 2009; Kwok, 2009).

The interplay between water masses and other influences that impact sea ice formation in the Barents Sea determine the position of the marginal ice zone, an area characterized by high surface productivity during the summer season (e.g. Smith and Sakshaug, 1990). Within the Barents Sea, enhanced primary production results from a peak algal bloom along the ice margin during spring as sea ice retreats (Sakshaug *et al*., 1992). In addition, the advection of

Atlantic Water contributes to longer productive seasons, compared to other Arctic areas (Wassmann, 2011). Consequently, the Barents Sea is one of the most productive areas of the Arctic Seas (Wassmann *et al*., 2006; Wassmann, 2011).

Material and methods

A 245 cm long marine sediment core NP05-11-70GC was retrieved in 2005 by the RV *Lance* south of Kong Karls Land (Olga Basin) within the northern Barents Sea (78.40° N, 32.42° E; 293 m water depth) using a gravity coring device (Fig. 1). The upper section of the core (0–124 cm; 1-cm intervals) was investigated in the current study and was characterized by homogeneous sediments rich in silty clay deposited in a marine environment.

Chronology

A depth-age model for NP05-11-70GC was developed using linear interpolation between three calibrated AMS ^{14}C dates obtained from mixed benthic foraminifera as described by Berben (2014) and Belt *et al*. (2015) (Fig. 2; Table 1; Table S2). In order to try and improve the age control, attempts to obtain more ^{14}C dates were made by collecting all benthic foraminifera at each core level selected for microfossil analyses (i.e. every cm). Unfortunately, additional ^{14}C measurements were prevented due to the very low numbers of foraminifera (and thus insufficient amounts of $CaCO_3$ (Fig. 4)). Nonetheless, the lithological description of a marine sediment core from a very nearby location in the northern Barents Sea also indicate a well-defined homogeneous unit corresponding to Holocene sediments (Klitgaard Kristensen *et al*., 2013). Thus, based on lithological similarities, together with some younger AMS ^{14}C dates (<2000 cal a BP) in a nearby core, the NP05-11-70GC core top is assumed to represent modern age. The AMS ^{14}C dates were calibrated using Calib 6.1.1 (Stuiver and Reimer, 1993) and the Marine09 calibration curve (Reimer *et al*., 2009). A local reservoir age (ΔR) of 105±24 suggested for the Svalbard area by Mangerud *et al*. (2006) was used in the calibration (Table 1).

Biomarker analysis

To reconstruct past sea ice conditions, the seasonal sea ice biomarker IP_{25} and the open water phytoplankton biomarkers (brassicasterol and HBI III) were analysed in 49 sub-samples (ca. 1 g taken from the same bulk sediment samples used for foraminiferal analysis). Prior to analysis, sub-samples were freeze-dried and stored at -20 °C. The general methodology for biomarker extraction, purification and analysis was as previously described by Belt *et al.* (2012) and Brown and Belt (2012). Analytical reproducibility was monitored using a sediment with known biomarker concentrations for every 10–12 extracted sediment samples (analytical error <6%, n=5). Lipid quantification was conducted using the integrated peak areas of each biomarker and the internal standard, an instrumental response factor, and the masses of the extracted sediment and internal standard (Belt *et al.,* 2012). Biomarker concentrations, normalized to dry weight sediment mass (µg/g sed.) as presented previously (Belt *et al*., 2015), were further normalized to total organic carbon (µg/g TOC) in order to compensate possible regional differences in production and degradation in sediments (Belt and Müller, 2013). The weight percentages (wt. %) of TOC (n=43) were determined using a Carlo Erba EA 1110 elemental analyzer at Plymouth University. In order to remove any inorganic carbonate, ca. 100 mg of freeze-dried sediment was digested in HCl (1mL; 18h).

To investigate past sea ice conditions more quantitatively, IP_{25} and phytoplankton biomarkers were used to calculate the so-called P_BIP_{25} and $P_{III}IP_{25}$ indices (i.e. PIP_{25} based on brassicasterol and HBI III, respectively) (Müller *et al.,* 2011; Belt *et al.,* 2015). Calculation of the P_BIP_{25} index was achieved using Eq. 1, which includes a concentration balance factor (*c*; Eq. 2) to compensate for the significant concentration difference between IP_{25} and brassicasterol (Müller *et al*., 2011).

$$P_BIP_{25} = IP_{25} / (IP_{25} + (\text{brassicasterol} * c)) \quad \text{[Eq. 1]}$$

$$c = \text{mean } IP_{25} / \text{mean brassicasterol} \quad \text{[Eq. 2]}$$

Calculation of $P_{III}IP_{25}$ indices was achieved by replacing brassicasterol concentrations (Eq. 1) with those of HBI III. The balance factor, *c*, was calculated according to the relative mean concentrations of IP_{25} and HBI III (i.e. as per brassicasterol; Eq. 2) and we also used a value of 0.63, derived from a regional calibration of surface sediments from the Barents Sea (Belt *et al*., 2015; Smik *et al*., 2016). In practice, $P_{III}IP_{25}$ values using a *c* term based on Eq. 2 (0.84) were very similar to those using the value of *c* derived from the surface sediment calibration (0.63; Smik *et al*., 2016). For simplicity, we present data using the surface sediment

calibration only. Semi-quantitative estimates of SpSIC were also made using the $P_{III}IP_{25}$ data and the calibration of Smik *et al*. (2016) (Eq. 3) (for more background information, see Introduction).

$$SpSIC\ (\%) = (P_{III}IP_{25} - 0.0692) / 0.0107 \qquad [Eq.\ 3]$$

Planktic foraminifera

The sediment core was opened, and the sediments were sampled and frozen within 48 hours. Sediment samples were freeze-dried, wet-sieved through three different size fractions (1000, 100 and 63 µm), and dried at 40 °C. Planktic foraminiferal assemblages were determined for 123 samples using the 100–1000 µm size fraction following Knudsen (1998). Following Forcino (2012), the relative abundances (%) of each species were calculated for samples containing more than 25 specimens (82 samples). Identification of *Neogloboquadrina pachyderma* and *Neogloboquadrina incompta* species was achieved following Cifelli (1961) and Darling *et al*. (2006), and planktic foraminiferal concentrations (#/g sed.) were calculated.

As the planktic foraminiferal assemblages might be affected by carbonate dissolution, it is important to assess the impact of preservation changes on the planktic foraminiferal data (e.g. Zamelczyk *et al.,* 2013). Here, the preservation conditions were investigated by analysing preservation indicators such as the mean shell weight of *N. pachyderma* and the percentage of fragmentation of planktic foraminiferal tests. A loss in the mean shell weight can be used to identify dissolution in the water column and sediment surface (Broecker and Clark, 2001; Barker and Elderfield, 2002; Barker *et al.,* 2004). Hence, 25 well preserved (visually) and square shaped *N. pachyderma* specimens were picked from each sample from a narrow size range (150–250 µm) in order to reduce problems of ontogeny and size difference induced variability (Barker *et al*., 2004). It was possible to obtain a mean shell weight (µg) of the 25 picked specimens per sample of *N. pachyderma* using a Mettler Toledo microbalance (0.1 µg sensitivity; 110 samples). Further, the degree of fragmentation indicates the dissolution induced weakening of the tests as well as dissolution processes within the sediment (Conan *et al*., 2002). The fragmentation (%) of planktic foraminiferal tests was calculated for the 82 samples that contained a total number of >25 specimens within the 100–1000 µm size fraction. The fragmentation was calculated using the equation proposed by Pfuhl and Shackleton (2004) (Eq. 4).

Fragmentation = ((#fragments/g) / ((#fragments/g/3) + (#tests/g))) * 10 [Eq. 4]

Stable carbon and oxygen isotope analysis

The stable carbon and oxygen isotopic compositions of planktic foraminiferal shells ($\delta^{18}O$, $\delta^{13}C$) are widely used to reflect the ambient sea water mass properties in which they have been calcified. In particular, $\delta^{18}O$ is a proxy for temperature and salinity, whereas $\delta^{13}C$ variations reflect primary production and stratification changes (e.g. Spielhagen and Erlenkeuser, 1994; Katz *et al.,* 2010). The $\delta^{18}O$ and $\delta^{13}C$ analyses were performed on the foraminiferal tests of *N. pachyderma*. All specimens were selected from a narrow size range (150–250 µm) in order to minimize size dependent effects on isotopic composition (Aksu and Vilks, 1988; Keigwin and Boyle, 1989; Oppo and Fairbanks, 1989; Donner and Wefer, 1994; Bauch *et al*., 2000). Sufficient amount of specimens were obtained from 105 samples. Samples were analysed using a Finnigan MAT 253 mass spectrometer coupled to an automated Kiel IV Carbonate Preparation Device at the Geological Mass Spectrometer (GMS) Laboratory at the University of Bergen. These measurements were conducted with a reproducibility of ±0.06 ‰ ($\delta^{18}O$) and ±0.03 ‰ ($\delta^{13}C$). Data are reported on the ‰ versus VPDB scale calibrated with NBS-19. Corrections for the ice volume effect were applied on the measured $\delta^{18}O$ values according to Fairbanks (1989). No vital effect corrections were applied for the isotope measurements in this study as published estimates of species-specific vital effects are often inconsistent (e.g. Kohfeld *et al*., 1996; Bauch *et al*., 1997; Stangeew, 2001; Simstich *et al*., 2003), possibly due to seasonal changes of the apparent vital effect (Jonkers *et al*., 2010).

Results

The resulting depth-age model ranges between the present and ca. 9400 cal a BP (Fig. 2). The depth-age model presented here has its limitations (for a detailed discussion, see Chronology) and hence, for this reason, assigned ages should be taken with caution. Therefore, all data plots presenting the results of this study also include a depth scale, although the results are described with respect to age to enable us to place them into a wider context, both spatially and temporally, when comparing them with previously published results. Despite the

limitations of the age control, which prevents the determination of centennial-scale changes, we believe it is nonetheless feasible to describe the general early to late Holocene changes with some confidence.

Biomarker data

The initial decrease in IP_{25} concentrations (2 data points) followed by low values, coincides with increased concentrations of both brassicasterol and HBI III ca. 9500–8500 cal a BP (Fig. 3a-c; Table S3). Hereafter, IP_{25} concentrations show slightly higher values, whereas brassicasterol and HBI III show decreased concentrations towards ca. 5900 cal a BP (Fig. 3a-c). During this entire time interval (i.e. ca. 9500–5900 cal a BP), a decreasing trend in TOC is also observed, although values remain relatively high (Fig. 3d; Table S3). From ca. 5900–2700 cal a BP, the concentration of IP_{25} increases further, while brassicasterol and HBI III both decrease although TOC values remain relatively stable (Fig. 3a-d). The last ca. 2700 cal a BP are characterized by the highest concentrations of IP_{25} and relatively low (but stable) concentrations of brassicasterol and HBI III (Fig. 3a-c). Although the TOC values fluctuate somewhat throughout this period, the absolute values are the lowest within the entire record (Fig. 3d).

Both P_BIP_{25} and $P_{III}IP_{25}$ indices, as well as the estimated SpSIC (which is linearly related to $P_{III}IP_{25}$; Smik *et al.,* 2016), follow the same trends throughout the entire record (Fig. 3e-g; Table S3). After the initial lowest values at ca. 9000 cal a BP, each of P_BIP_{25}, $P_{III}IP_{25}$ and SpSIC show increasing (although still relatively low) values towards ca. 5900 cal a BP (Fig. 3e-g). The mean SpSIC estimate ca. 9500–5900 cal a BP is ca. 25% (Fig. 3g). From ca. 5900–2700 cal a BP, the P_BIP_{25}, $P_{III}IP_{25}$ and SpSIC records continue their increasing trend, albeit more gradually. The estimated SpSIC shows a mean value of ca. 60% throughout this time interval (Fig. 3g) with highest values towards ca. 2700 cal a BP. The P_BIP_{25} reaches its highest value at the core top, whereas the $P_{III}IP_{25}$ records a maximum value at ca. 1600 cal a BP after which it remains high until the present (Fig. 3e-f). Estimates of SpSIC show a mean value of ca. 75% (Fig. 3g). According to the threshold limit ($P_{III}IP_{25}$>0.8) suggested by Smik *et al.* (2016), the occurrence of summer sea ice (SuSIC>5%) is estimated to have begun ca. 2700 cal a BP and remained a consistent feature thereafter, until the present (Fig. 3f).

Planktic foraminiferal preservation

From ca. 9500–7300 cal a BP, the absolute abundances of planktic foraminifera remain relatively low where after, they increase towards 5900 cal a BP (Fig. 4a; Table S4). From ca. 5900–2700 cal a BP, the planktic foraminiferal concentration has a broader range (Fig. 4a), while in the last ca. 2700 cal a BP, three episodes of increased planktic foraminiferal concentration values are observed ca. 2400–2000 cal a BP, ca. 1600–700 cal a BP, and ca. 400 cal a BP–present (Fig. 4a).

From ca. 9500–5900 cal a BP, the extent of fragmentation shows a mean value of 32%, whereas the mean shell weight is highly variable until ca. 7300 cal a BP, followed by more stable values (ca. 7.5 µg) towards ca. 5900 cal a BP (Fig. 4b-c; Table S4). The mean shell weight remains relatively stable (ca. 7 µg) ca. 5900–2700 cal a BP, while the fragmentation record exhibits an overall decrease (Fig. 4b-c). During the last ca. 2700 cal a BP, the degree of fragmentation shows a small overall increase although there is mainly an increase in the amplitude (i.e. minima and maxima between ca. 9–83%) (Fig. 4b). At the same time, the mean shell weight shows a general decrease (Fig. 4c).

Planktic foraminiferal fauna

The planktic foraminiferal record is characterized by the presence of polar (*N. pachyderma*) and sub-polar (*N. incompta*, *Turborotalita quinqueloba*, *Globigerinita glutinata*, *Globigerina bulloides* and *Globigerinita. uvula*) species with *N. pachyderma* generally dominating the assemblages (Fig. 4d-i; Table S4). From ca. 9500–7300 cal a BP, the fauna is dominated by *N. pachyderma* (ca. 95%) followed by a period (ca. 7300–5900 cal a BP) with increased relative abundances of *T. quinqueloba, N. incompta* and *G. glutinata* up to ca. 24, 27 and 4%, respectively (Fig. 4d-g). After ca. 5900 cal a BP, the relative abundances of *T. quinqueloba* and *N. incompta* decrease and remain relatively stable (ca. 3–4%) towards ca. 2700 cal a BP, while *N. pachyderma* clearly dominates the planktic foraminiferal fauna (Fig. 4d-f). Throughout the last ca. 2700 cal a BP, a reduction in *N. pachyderma* (towards ca. 65%) is accompanied by increasing relative abundances of *G. glutinata* (ca. 5%) and *G. bulloides* (ca. 8%), whereas *T. quinqueloba* and *N. incompta* reach their highest values between ca. 2400–2000 cal a BP, ca. 1600–700 cal a BP and ca. 400 cal a BP–present (Fig. 4d-h). The period

from ca. 400 cal a BP–present is characterized by a clear increase of *G. glutinata* (ca. 7%) and *G. bulloides* (ca. 6%), in addition to a remarkable increase of *G. uvula* (ca. 7%) (Fig. 4g-i).

Stable carbon and oxygen isotope data

From ca. 9500–8800 cal a BP, the $\delta^{18}O$ (*N. pachyderma*) record has a mean value of 3.8 ‰ followed by a period (ca. 8800–7300 cal a BP) characterized by lighter values (Fig. 5a; Table S5). A significant increase in $\delta^{18}O$ ca. 7600–7300 cal a BP is followed by heavier values that fluctuate around ca. 3.7 ‰ until ca. 5900 cal a BP. The $\delta^{18}O$ record remains relatively stable ca. 5900–2700 cal a BP with relatively heavy values (Fig. 5a). Throughout the last ca. 2700 cal a BP, the $\delta^{18}O$ record shows decreased values in the range 3.5–4.0 ‰ (Fig. 5a).

The $\delta^{13}C$ record shows a decrease from 0.4 to 0.0 ‰ ca. 9500–8500 cal a BP (Fig. 5b; Table S5). This trend is reversed at ca. 8500 cal a BP, with heavier $\delta^{13}C$ values towards ca. 5900 cal a BP followed by an increase towards 0.9 ‰ ca. 5900–2700 cal a BP (Fig. 5b). The last ca. 2700 cal a BP are then characterized by a decreasing trend with $\delta^{13}C$ values in the range 0.3–0.8 ‰ (Fig. 5b).

Discussion

Throughout the early to late Holocene, the palaeoceanographic record in NP05-11-70GC shows an overall increase in sea ice reflecting the decline in solar insolation (Fig. 6a-d). Related IP25-based reconstructions have been reported for other Arctic and sub-Arctic regions such as the Fram Strait, the Laptev Sea, the East Siberian Sea and the Chukchi Sea (Stein *et al.,* 2016a), as well as for the Canadian Arctic (Vare *et al.,* 2009; Belt *et al.,* 2010) and North Iceland (Cabedo-Sanz *et al.,* 2016b). However, for some other regions, including the Alaskan margin (Polyak *et al.,* 2016) and the western Barents Sea (Berben *et al.,* 2014), this long-term trend is not as evident. The record presented here for the northern Barents Sea is described in terms of individual time intervals reflecting the main stages of sea ice conditions and Atlantic Water inflow. The intervals are: Period I (ca. 9500–5900 cal a BP), Period II (ca. 5900–2700 cal a BP) and Period III (ca. 2700 cal a BP–present), although the interpretation of the timing of the exact boundaries between these intervals should be considered with caution due to the limitations of the age-depth model (see Chronology).

Climate and oceanographic variations during these periods are discussed and set into further context by comparison with previously published records from the region.

Our interpretation of the sea ice conditions involves the identification of previously unavailable semi-quantitative estimates of SpSIC and summer sea ice occurrence using a recently calibrated biomarker approach, which has also permitted the proposal of different sea ice scenarios. To obtain realistic representations for such sea ice conditions, known scenarios derived from modern and historical observations of the Barents Sea (NSIDC) have been considered (Fig. 1b). For example, the modern sea ice conditions have been derived from maximum (March) and seasonal variability (April/August) in sea ice using satellite data obtained between 1981 and 2010 (NSIDC) (Fig. 7c). In terms of temporal changes, historical data from the Barents Sea show variations in the mean sea ice margin position in April for four sub-periods between 1870 and 2002 (Divine and Dick, 2006). A north-easterly retreat of the sea ice margin since the second half of the 19th century occurred after a significant cooling in the second half of the 18th century (Divine and Dick, 2006) (Fig. 1b). This historical data from the Barents Sea illustrates that the decadal migration pattern of the sea ice margins associated with climatic conditions can reflect observed sea ice changes on an annual and/or seasonal time scale. Therefore, this key dataset provides precedent for the proposed sea ice scenarios (and changes to these) within the Barents Sea during the early to late Holocene.

With respect to the planktic foraminiferal preservation conditions, the proxy data is interpreted as follows. Better calcium carbonate preservation has been associated with increased production of organic matter in regions impacted by Atlantic Water (e.g. Hebbeln *et al.* 1998; Henrich *et al.* 2002). In particular, for areas with enhanced Atlantic Water inflow towards the Fram Strait, ocean currents appear to have a positive influence on the preservation of organic matter in sediments (Birgel and Stein, 2004; Birgel *et al.,* 2004). The wide range in both fragmentation and mean shell weight could therefore reflect variable environmental control, preservation conditions or a combination of both. The high mean shell weight ca. 7300–5900 cal a BP indicates better preservation conditions, possibly related to an increased influence of Atlantic Water (Fig. 4c). In contrast, throughout the last ca. 2700 cal a BP, the preservation indicators (i.e. low mean shell weight and highly fluctuating fragmentation) show an overall change towards enhanced dissolution (Fig. 4b-c). This may be caused by an increased influence of sea ice formation and brine rejection which may form corrosive bottom water masses causing dissolution at the sea floor (e.g. Midttun 1985; Steinsund and Hald 1994). Further, the low planktic foraminiferal concentrations may seem to

indicate poor preservation conditions, however studies of recent planktic foraminifera show that low planktic foraminiferal concentrations can be found within environments characterized by sea ice conditions (Carstens *et al.* 1997; Pados and Spielhagen 2014). In addition, the data in this study is consistent with planktic foraminiferal concentrations from the Barents Sea region (e.g. Klitgaard Kristensen *et al.* 2013; Duplessy *et al.* 2001). When compared with other studies from the region (e.g. Zamelczyk *et al.* 2012, 2013; Berben *et al.* 2014), however, the current fragmentation and mean shell weight data indicate good preservation, especially throughout the early part of the record. Therefore, the generally low planktic foraminiferal concentrations are attributed here to the environmental conditions such as the shallow shelf environment influenced by Arctic Water with a reduced salinity and the proximity of the sea ice margin.

Regarding the planktic foraminiferal oxygen isotope signal, studies of recent foraminiferal calcite and the isotopic composition of water masses by Lubinski *et al.* (2001) demonstrate that, in the Barents Sea, these are controlled mainly by temperature changes rather than salinity. However, the water masses in the region are also influenced by meltwater and reduced salinities, especially during the earliest part of the Holocene, although this influence probably diminished around ca. 11 000 cal a BP (Klitgaard Kristensen *et al.,* 2013). Therefore, it is further assumed that the stable isotope record has been mainly controlled by temperature.

Period I (ca. 9500–5900 cal a BP): minimum sea ice conditions with reduced SpSIC (ca. 25%)

During Period I, low IP_{25} concentrations reflect reduced seasonal sea ice, while high brassicasterol and HBI III concentrations are indicative of open water and sea ice margin conditions, respectively (Fig. 3a-c). At the same time, the lowest P_BIP_{25} and $P_{III}IP_{25}$ values indicate reduced spring sea ice conditions, with longer (warmer) summers suitable for phytoplankton production (Müller *et al.,* 2011; Belt *et al*., 2015; Smik *et al*., 2016) (Fig. 3e-f), which is also reflected by the generally higher TOC values (Fig. 3d). Maximum HBI III concentrations indicate decreasing winter ice margin conditions from ca. 9500–8500 cal a BP (Belt *et al*., 2015), with SpSIC estimates consistently less than 50% (mean ca. 25%) (Fig. 3g) and an absence of summer sea ice (Fig. 3f-g). The occurrence of reduced SpSIC and longer (ice-free) summers is consistent with longer ice-free seasons and a retreated ice margin

observed in the northern Barents Sea (Duplessy *et al*., 2001) and increased phytoplankton production in the northern Fram Strait (Müller *et al*., 2009, 2012) (for location of these study sites please refer to Fig. 1). Reduced spring sea ice conditions likely indicate the occurrence of the Holocene Thermal Maximum as recorded at the sea surface ca. 9300–6500 cal a BP. The subsequent increase in IP_{25} concentration after ca. 6500 cal a BP reflects a general enhancement in sea ice conditions probably marking the gradual transition of the Holocene Thermal Maximum towards Neoglacial conditions (Fig. 6b). Similar conclusions regarding timing and termination of the Holocene Thermal Maximum based on IP_{25} records have been made for the Fram Strait (until ca. 8400 cal a BP; (Müller *et al*., 2009)) and the West Svalbard margin, where the last phase of the Holocene Thermal Maximum was recorded ca. 8500–7000 cal a BP (Müller *et al*., 2012). Furthermore, the observed disappearance of sea ice in the western Barents Sea from ca. 10 700–7700 cal a BP has been linked previously to the Holocene Thermal Maximum (Sarnthein *et al.,* 2003).

The light $\delta^{18}O$ (*N. pachyderma*) values ca. 8800–7300 cal a BP indicate a small temperature rise, possibly reflecting a gradual shift towards a warmer sub-surface water mass due to increased Atlantic Water inflow (Fig. 6e). The relatively light $\delta^{18}O$ values also coincide with high insolation, thereby reflecting the Holocene Thermal Maximum at the core site (Fig. 6e). The strong increase in $\delta^{18}O$ values ca. 7600–7300 cal a BP probably reflects its termination, a conclusion consistent with observations of Duplessy *et al*. (2001) for a nearby location. Furthermore, Hald *et al.* (2007) presented a time-transgressive Atlantic Water inflow from south to north along the Norwegian and Svalbard margins. Risebrobakken *et al.* (2011) suggested that this time-transgressive northward intensified heat advection resulted from major reorganization of the ocean circulation following the deglaciation. Hence, throughout the Holocene Thermal Maximum, high latitude radiative forcing was not responsible for the overall conditions of the water column and ocean dynamics, although it might have further enhanced the transport of warm salty water (Risebrobakken *et al.,* 2011). Within the broader study area, Lubinski *et al*. (2001) associated decreasing $\delta^{18}O$ values ca. 10 000–6800 cal a BP with a possible increase of surface water temperatures due to a return inflow of warm water. A stronger Atlantic Water inflow delivered by the Svalbard Branch has also been recorded at the western and northern Svalbard margins ca. 8000 cal a BP (Slubowska *et al*., 2005; Werner *et al*., 2013) and in the Franz Victoria Trough ca. 7500 cal a BP (Duplessy *et al*., 2001). However, since the $\delta^{18}O$ values do not correspond to the observed time-transgressive pattern of the Svalbard Branch, it is assumed that the core site was influenced by Atlantic Water

inflow entering the Barents Sea via the North Cape Current. This is consistent with decreased $\delta^{18}O$ observations in the southern Barents Sea ca. 11 000–9800 cal a BP (Risebrobakken *et al*., 2010), the western Barents Sea ca. 10 000 cal a BP (Berben *et al*., 2014) and the north-western Barents Sea ca. 7000 cal a BP (Klitgaard Kristensen *et al*., 2013) (for study locations please refer to Fig. 1).

During Period I, the overall high relative abundances of *N. pachyderma*, in particular ca. 9500–7300 cal a BP, suggest a dominance of Arctic Water masses and cold conditions at the study site (Volkmann, 2000). However, from ca. 7300–5900 cal a BP, the increased abundances of sub-polar species as well as of total planktic foraminifera indicate a pronounced influence of relatively warm Atlantic Water inflow at the core site (Bé and Tolderlund, 1971; Johannessen *et al*., 1994; Carstens *et al*., 1997) (Fig. 6f-g). Correspondingly, elevated planktic foraminiferal concentrations were recorded in the north-eastern Barents Sea and linked to an intrusion of Atlantic Water (Duplessy *et al.,* 2001). Similar interpretations were made for the northern Barents Sea (Klitgaard Kristensen *et al.,* 2013) and the western Barents Sea (Sarnthein *et al.,* 2003; Berben *et al.,* 2014).

Nonetheless, the timing of changes in Atlantic Water inflow based on planktic foraminiferal assemblages (ca. 7300–5900 cal a BP) differs from that based on $\delta^{18}O$ (ca. 8800–7300 cal a BP). In the Arctic Ocean, the calcification of *N. pachyderma* is linked to phytoplankton blooms occurring mainly in August (Kohfeld *et al.,* 1996; Volkmann, 2000), whereas the planktic foraminiferal fauna reflects an annual signal. Additionally, sea ice conditions can result in a shift in the growing season (e.g. Farmer *et al.,* 2008) and a species-specific change in its calcification depth. Therefore, the $\delta^{18}O$ of *N. pachyderma* reflects a different temperature compared to the total foraminiferal assemblage (Simstich *et al.,* 2003) and might reflect a different signal with respect to seasonality and/or water depth. Furthermore, the faunal response depends on more factors than temperature and salinity. For example, *T. quinqueloba* also depends on the available food supply (e.g. Volkmann, 2000) and is characteristic of Arctic Front conditions in the western Barents Sea (Burhol, 1994). An increased nutrition availability associated with oceanic front conditions might have followed later in time. Indeed, such a delay in food supply is suggested by increasing $\delta^{13}C$ values ca. 7300–5800 cal a BP which likely reflect enhanced primary production, possibly associated with increased seasonal sea ice conditions, as suggested from the IP_{25} data. Hence, the timing of increased relative abundances of sub-polar species is probably related to a combination of

enhanced Atlantic Water inflow and increased nutrition availability, as seen previously in the northern Barents Sea (Duplessy *et al.,* 2001).

For Period I, the new proxy data, combined with outcomes from previous studies, indicate that the study site was characterized by reduced sea ice conditions during relatively short spring seasons, enhanced phytoplankton production within the proximity of the sea ice margin, and a winter sea ice margin in the proximity of the core site at ca. 78° N (Fig. 7a). These sea surface conditions were likely influenced by maximum insolation, while the sub-surface water masses were probably controlled more by oceanic dynamics (Andersson *et al.,* 2010; Risebrobakken *et al.,* 2011). In particular, a time-transgressive Atlantic Water inflow resulted in initially cold water masses followed by warmer Atlantic Water at the study site. The strengthening of Atlantic Water inflow might have additionally contributed to the reduced sea ice conditions as seen during modern times in the Barents Sea (Årthun *et al*., 2012). Such a proposed sea ice scenario implies that water masses south of the study area were ice free, consistent with open water conditions observed in the western Barents Sea (Sarnthein et al., 2003; Berben *et al*., 2014) and the West Svalbard margin (Müller *et al*., 2012) (Fig. 7a) during the early Holocene.

Period II (ca. 5900–2700 cal a BP): marginal ice zone conditions with increasing SpSIC (ca. 60%)

Throughout Period II, higher IP_{25} concentrations and parallel decreases in brassicasterol and HBI III concentrations reflect increased seasonal sea ice with less open water conditions (Fig. 3a-c). Increasing P_BIP_{25} and $P_{III}IP_{25}$ values indicate marginal ice zone conditions at the study site (Müller *et al*., 2011; Belt *et al*., 2015) (Fig. 3e-f) with a mean SpSIC of ca. 60% but increasing throughout this interval to ca. 70% (Fig. 6d). Despite a general increase in SpSIC, however, the $P_{III}IP_{25}$ data suggest that the site was probably ice free throughout the summer months (Smik *et al.,* 2016) (Fig. 6c). Similar IP_{25}-based reconstructions of sea ice conditions have been attributed to mid Holocene Neoglacial cooling for the northern Fram Strait (Müller *et al*., 2009) and the West Svalbard margin (Müller *et al*., 2012).

The heavy $\delta^{18}O$ (*N. pachyderma*) values during Period II indicate lower temperatures and a decreased influence of Atlantic Water (Fig. 6e), consistent with previous observations from the region (Duplessy *et al*., 2001; Klitgaard Kristensen *et al*., 2013). It has also been

suggested that Arctic Water from the north-eastern Barents Sea might have influenced the western Barents Sea due to less heat advection from the south (Hald *et al*., 2007).

The dominance of *N. pachyderma*, along with decreased abundances of sub-polar foraminifera, such as *T. quinqueloba* and *N. incompta* indicate the prevailing presence of colder Arctic Water at the core site (Volkmann, 2000) (Fig. 6f-g). This is consistent with foraminifera-based observations of cold conditions after ca. 5200 cal a BP in the eastern Fram Strait (Werner *et al.,* 2013) and reduced Atlantic Water inflow in the western Barents Sea (Sarnthein *et al.,* 2003).

Combined, the biomarker and microfossil proxy data indicate a continuous cooling trend during Period II with a dominance of cold Arctic Water and an accompanying increase in SpSIC, likely as a result of decreasing summer insolation and a cooler surface water layer. Consequently, the strongly reduced Atlantic Water inflow could not have affected the sea ice conditions in the same way as was proposed for Period I. In addition, our data suggest that the maximum winter sea ice margin was probably located ca. 76–77° N or, at least, further south compared to the Period I (Fig. 7a-b). This is in good agreement with sea ice conditions at the continental slope of western Svalbard (Müller *et al*., 2012), although sea ice did not extend as far as the western Barents Sea (Berben *et al*., 2014) (Fig. 7b). With respect to the position of the summer sea ice margin, the increased $P_{III}IP_{25}$ values also suggest a location further south compared to Period I, consistent with previous observations in the northern Barents Sea after ca. 6000 cal a BP (Duplessy *et al.,* 2001; Klitgaard Kristensen *et al.,* 2013) (Fig. 7b).

Period III (ca. 2700 cal a BP–present): Arctic frontal conditions with high SpSIC (ca. 75%) and summer sea ice

Increases to IP_{25}, P_BIP_{25} and $P_{III}IP_{25}$ reflect further increases in spring sea ice conditions during Period III (Fig. 3a; e-f), while lower brassicasterol and HBI III concentrations indicate less open water phytoplankton production consistent with lower TOC values (Fig. 3b-d). These results point to Arctic frontal conditions that are similar to the modern setting (Müller *et al.,* 2011; Belt *et al.,* 2015). Indeed, the $P_{III}IP_{25}$-based SpSIC estimates (ca. 75%) align closely with contemporary values derived from satellite records (Smik *et al*., 2016) (Fig. 6c-d), while $P_{III}IP_{25}$ values generally >0.8 are also indicative of the occurrence of summer sea ice (Smik *et al.,* 2016), also a feature of the modern setting. Consistent with these findings,

extended sea ice conditions have been reported for the Fram Strait for the last ca. 3000 cal a BP (Müller *et al.,* 2012).

The mainly light, but variable, $\delta^{18}O$ (*N. pachyderma*) values, are most likely indicative of a generally increased influence of Atlantic Water inflow (Fig. 6e), consistent with previous reports of episodic increases in Atlantic Water for the northern Barents Sea (Duplessy *et al*., 2001; Lubinski *et al*., 2001), the western Barents Sea (Wilson *et al*., 2011; Berben *et al*., 2014) and the Svalbard margin (Jernas *et al*., 2013; Werner *et al*., 2013) during the late Holocene.

The decrease in *N. pachyderma* and increased relative abundance of sub-polar foraminifera, especially *G. bulloides*, which is usually associated with the warmest parts of the Norwegian Atlantic Current (Johannessen *et al*., 1994) also reflect the generally increasing influence of Atlantic Water during this period (Fig. 6f-g). However, the fluctuations in the faunal data throughout Period III still indicate variability in the influence of Atlantic Water consistent with previous findings from the western Barents Sea (Sarnthein *et al.,* 2003).

The increase in sea ice conditions reflects an overall cooling trend recorded previously in various Arctic terrestrial (e.g. Bjune *et al*., 2009; Kaufman *et al*., 2009), ice core (e.g. Kaufman *et al*., 2009; Divine *et al*., 2011) and marine records (e.g. Slubowska *et al*., 2005; Skirbekk *et al*., 2010), likely resulting from lower insolation affecting the sea surface. A negative solar irradiance anomaly ca. 2850–2600 cal a BP may also have resulted in decreased ventilation of the sub-surface waters, as corroborated by modelling experiments (Renssen *et al*., 2006). Meanwhile, the increased influence of Atlantic Water inflow might be attributed to stronger stratification among the upper layers as seen in previous studies of the Barents Sea (Lubinski *et al*., 2001; Duplessy *et al*., 2005; Risebrobakken *et al*., 2010; Wilson *et al*., 2011) and the Svalbard margin (Jernas *et al*., 2013; Werner *et al*., 2013).

The occurrence of sea surface cooling and sub-surface warming indicates that Period III was most likely characterized by a strong vertical stratification and a decoupling between the atmosphere and the oceanic sub-surface. Summer insolation was at its lowest during Period III (Fig. 6a), resulting in cooler atmospheric temperatures and potentially enhanced sea ice production and/or reduced sea ice melt. In addition to the stronger vertical stratification of the water column, the increased sea ice conditions probably also limited the heat exchange between the atmosphere and the sub-surface water masses. In terms of seasonality, we suggest that relatively long spring seasons with extensive sea ice conditions would have been

accompanied by shorter (and probably cooler) summers with lower phytoplankton production (Fig. 7c). Overall, the site was characterized by extensive sea ice conditions (SpSIC typically ca. 75%) with at least partial sea ice occurrence in the summer months (Fig. 7c). Such interpretations are also consistent with previous qualitative reports of intensified sea ice occurrence in the northern Barents Sea (Duplessy *et al*., 2001; Klitgaard Kristensen *et al*., 2013), increasing sea ice conditions in the Fram Strait (Müller *et al*., 2009, 2012; Werner *et al.,* 2014) and in the western Barents Sea throughout the last ca. 1100 cal a BP (Berben *et al*., 2014). Hence, the data suggest a south-westwards transgression of the sea ice margin (Fig. 7c). Finally, the sea ice conditions most likely exceeded the modern sea ice margin during the (pre-industrial) late Holocene (Fig. 7c). A slight reversal in the extent of spring sea ice conditions during recent decades and a return to more open water conditions during summer (c.f. Period II) is evident during the last ca. 100 yr from observational records (Divine and Dick, 2006).

Conclusions

Early to late Holocene semi-quantitative estimates of SpSIC and the qualitative occurrence of summer sea ice in the northern Barents Sea have been reconstructed based on the variability of source-specific biomarkers within a marine sediment core taken from the Olga Basin. Additional proxy data based on planktic foraminifera that reflect the sub-surface water masses have demonstrated the evolution of Atlantic Water inflow to the Barents Sea. The major palaeoceanographic evolution can be summarised as follows: During Period I (ca. 9500–5900 cal a BP), reduced SpSIC (ca. 25%) was controlled, primarily, by relatively high summer insolation. The core site was also influenced by Atlantic Water entering the Barents Sea via the North Cape Current which caused an increased heat exchange between the ocean and the atmosphere and likely contributed to reduced sea ice conditions. The site was probably located close to the maximum winter sea ice margin, such that it experienced only relatively short periods of sea ice during the spring together with long (ice-free) productive summers.

An overall cooling trend characterized Period II (ca. 5900–2700 cal a BP), with increased SpSIC (ca. 60%) and delivery of cold Arctic Water. This interval was also characterized by a general southward advance of the winter and summer sea ice margins, although, summer months were still ice free.

Period III (ca. 2700 cal a BP–present) was marked by extensive SpSIC (ca. 75%), partial summer sea ice occurrence and increased Atlantic Water inflow. Increased sea ice conditions were probably induced by progressively lower insolation, while sub-surface warming due to increased Atlantic Water demonstrates a likely decoupling between the atmosphere and the ocean. The maximum winter sea ice margin was probably at its most southerly location within the record, with long spring seasons of extensive sea ice conditions followed by shorter and less productive summers. A slight retreat in the position of the winter sea ice margin is proposed for recent decades based on observational records.

Supporting information

Additional supporting information related to this article may be found in the online version of this article.

Table S1. CTD data presented in Fig. 1

Table S2. Age model presented in Fig. 2

Table S3. Biomarker data presented in Fig. 3

Table S4. Foraminiferal fauna data presented in Fig. 4

Table S5. Stable isotope data presented in Fig. 5

Acknowledgements. All data used in this work can be found in the supporting information for this paper. This work was carried out within the framework of the Initial Training Network program "Changing Arctic and Subarctic Environments" (CASE, Grant Agreement No. 238111) funded by the European Commission within the 7th Framework Program People, the Research Council of Norway in addition to UiT–The Arctic University of Norway and the Norwegian Polar Institute. Steffen Aagaard-Sørensen received financial support from the GlaciBar (Glaciations in the Barents Sea area) project funded by the Norwegian Research Council (NRC grant 200672/S60), Statoil, Det Norske and BG Norge. Thanks are also extended to Trine Dahl and Julia Sen for assisting with laboratory work in addition to Patricia Cabedo-Sanz for valuable discussions. Finally, we thank Ruediger Stein and one anonymous reviewer for their constructive feedback improving this manuscript.

References

Abrahamsen E, Østerhus S, Gammelsrød T. 2006. Ice draft and current measurements from the north-western Barents Sea, 1993-96. *Polar Research* **25**: 25-37.

Aksenov Y, Bacon S, Coward AC, Nurser AJG. 2010. The North Atlantic inflow to the Arctic Ocean: high-resolution model study. *Journal of Marine Systems* **79**: 1-22.

Aksu AE, Vilks G. 1988. Stable isotopes in planktonic and benthic foraminifera from Arctic Ocean surface sediments. *Canadian Journal of Earth Sciences* **25**: 701-709.

Andersson C, Pausata FSR, Jansen E, Risebrobakken B, Telford RJ. 2010. Holocene trends in the foraminifer record from the Norwegian Sea and the North Atlantic Ocean. *Climate of the Past* **6**: 179-193.

Barker S, Elderfield H. 2002. Foraminiferal calcification response to glacial interglacial changes in atmospheric CO_2. *Science* **297**: 883-836.

Barker S, Kiefer T, Elderfield H. 2004. Temporal changes in North Atlantic circulation constrained by planktonic foraminiferal shell weights. *Paleoceanography* **19**: PA3008.

Bauch D, Carstens J, Wefer G. 1997. Oxygen isotope composition of living Neogloboquadrina pachyderma (sin.) in the Arctic Ocean. *Earth and Planetary Science Letters* **146**: 47-58.

Bauch D, Carstens J, Wefer G, Thiede J. 2000. The imprint of anthropogenic CO_2 in the Arctic Ocean: evidence from planktic $d^{13}C$ data from water column and sediment surfaces. *Deep-Sea Research Pt. II* **9-11**: 1791-1808.

Bé AWH, Tolderlund DS. 1971. Distribution and ecology of living planktonic foraminifera in surface waters of the Atlantic and Indian Oceans. In *The micropaleontology of oceans,* Funnel BM, Riedel WR (eds). Cambridge University Press: London; 105-149.

Belt ST, Massé G, Rowland SJ, Poulin M, Michel C, LeBlanc B. 2007. A novel chemical fossil of palaeo sea ice: IP_{25}. *Organic Geochemistry* **38**: 16-27.

Belt ST, Vare LL, Massé G, Manners HR, Price JC, MacLachlan SE, Andrews JT, Schmidt S. 2010. Striking similarities in temporal changes to spring sea ice occurrence across the central Canadian Arctic Archipelago over the last 7000 years. *Quaternary Science Reviews* **29**: 3489-3504.

Belt ST, Brown TA, Navarro Rodriguez A, Cabedo Sanz P, Tonkin A, Ingle R. 2012. A reproducible method for the extraction, identification and quantification of the Arctic sea ice proxy IP_{25} from marine sediments. *Analytical Methods* **4**: 705-713.

Belt ST, Müller J. 2013. The Arctic sea ice biomarker IP_{25}: a review of current understanding, recommendations for future research and applications in palaeo sea ice reconstructions. *Quaternary Science Reviews* **79**: 9-25.

Belt ST, Cabedo-Sanz P, Smik L, Navarro-Rodriguez A, Berben SMP, Knies J, Husum K. 2015. Identification of paleo Arctic winter sea ice limits and the marginal ice zone: Optimised biomarker-based reconstructions of late Quaternary Arctic sea ice. *Earth and Planetary Science Letters* **431**: 127-139.

Berben SMP. 2014. *A Holocene palaeoceanographic multi-proxy study on the variability of Atlantic water inflow and sea ice distribution along the pathway of Atlantic water.* The Arctic University of Norway (PhD thesis).

Berben SMP, Husum K, Cabedo-Sanz P, Belt ST. 2014. Holocene sub-centennial evolution of Atlantic water inflow and sea ice distribution in the western Barents Sea. *Climate of the Past* **10**: 181-198.

Berger A. 1978. Long-term variations of daily insolation and quaternary climatic changes. *Journal of Atmospheric Sciences* **35**: 2363-2367.

Birgel D, Stein R. 2004. Northern Fram Strait and Yermak Plateau: Distribution, variability and burial of organic carbon and paleoenvironmental implications. In *The organic carbon cycle in the Arctic Ocean,* Stein R, Macdonald RW (eds). Springer-Verlag: Berlin; 279-295.

Birgel D, Stein R, Hefter J. 2004. Aliphatic lipids in recent sediments of the Fram Strait/Yermak Plateau (Arctic Ocean): composition, sources and transport processes. *Marine Chemistry* **88**: 127-160.

Bjune AE, Seppä H, Birks HJB. 2009. Quantitative summer temperature reconstructions for the last 2000 years based on pollen-stratigraphical data from northern Fennoscandia. *Journal of Paleolimnology* **41**: 43-56.

Broecker WS, Clark E. 2001. An evaluation of Lohmann's foraminifera weight dissolution index. *Paleoceanography* **16**: 531-534.

Brown TA, Belt ST, Philippe B, Mundy CJ, Massé G, Poulin M, Gosselin M. 2011. Temporal and vertical variations of lipid biomarkers during a bottom ice diatom bloom in the Canadian Beaufort Sea: Further evidence for the use of the IP_{25} biomarker as a proxy for spring Arctic sea ice. *Polar Biology* **34**: 1857-1868.

Brown TA, Belt ST. 2012. Identification of the sea ice diatom biomarker IP_{25} in Arctic benthic macrofauna: Direct evidence for a sea ice diatom diet in Arctic heterotrophs. *Polar Biology* **35**: 131-137.

Brown TA, Belt ST, Tatarek A, Mundy CJ. 2014. Source identification of the Arctic sea ice proxy IP_{25}. *Nature Communications* **5**: 4197.

Burhol ALS. 1994. *Recent distribution of planktonic foraminifera on the Svalbard-Barents margin.* University of Tromsø (Master thesis).

Cabedo-Sanz P, Belt ST, Knies J, Husum K. 2013. Identification of contrasting seasonal sea ice conditions during the Younger Dryas. *Quaternary Science Reviews* **79**: 74-86.

Cabedo-Sanz P, Belt ST. 2016a. Seasonal sea ice variability in eastern Fram Strait over the last 2000 years. *Arktos* **2(22)**: 1-12.

Cabedo-Sanz P, Belt ST, Jennings AE, Andrews JT, Geirsdóttir Á. 2016b. Variability in drift ice export from the Arctic Ocean to the North Icelandic Shelf over the last 8,000 years: a multi proxy evaluation. *Quaternary Science Reviews* **146**: 99-115.

Carmack E, Barber D, Christensen J, Macdonald R, Rudels B, Sakshaug E. 2006. Climate variability and physical forcing of the food webs and the carbon budget on panarctic shelves. *Progress in Oceanography* **71**: 145-181.

Carstens J, Hebbeln D, Wefer G.1997. Distribution of planktic foraminifera at the ice margin in the Arctic (Fram Strait). *Marine Micropaleontology* **29**: 257-269.

Cifelli R. 1961. Globigerina incompta, a new species of pelagic foraminifera from the North Atlantic. *Contributions Cushman Foundation Foraminiferal Research* **12**: 83-86.

Conan SMH, Ivanova EM, Brummer G-JA. 2002. Quantifying carbonate dissolution and calibration of foraminiferal dissolution indices in the Somali Basin. *Marine Geology* **182**: 325-349.

Darling KF, Kucera M, Kroon D, Wade CM. 2006. A resolution for the coiling direction paradox in Neogloboquadrina pachyderma. *Paleoceanography* **21**: PA2011.

Divine DV, Dick C. 2006. Historical variability of sea ice edge position in the Nordic Seas. *Journal Geophysical Research* **111**: C01001.

Divine D, Isaksson E, Martma T, Meijer HAJ, Moore J, Pohjola V, van de Wal RSW, Godtliebsen F. 2011. Thousand years of winter surface air temperature variations in Svalbard and northern Norway reconstructed from ice-core data. *Polar Research* **30**: 7379.

Donner B, Wefer G. 1994. Flux and stable isotope composition of Neogloboquadrina pachyderma and other planktonic foraminifers in the Southern Ocean (Atlantic sector). *Deep-Sea Research Pt. I* **41**: 1733-1743.

Duplessy JC, Ivanova E, Murdmaa I, Paterne M, Labeyrie L. 2001. Holocene paleoceanography of the northern Barents Sea and variations of the northward heat transport by the Atlantic Ocean. *Boreas* **30**: 2-16.

Duplessy JC, Cortijo E, Ivanova E, Khusid T, Labeyrie L, Levitan M, Murdmaa I, Paterne M. 2005. Paleoceanography of the Barents Sea during the Holocene. *Paleoceanography* **20**: A4004.

Ellingsen I, Slagstad D, Sundfjord A. 2009. Modification of water masses in the Barents Sea and its coupling to ice dynamics: A model study. *Ocean Dynamics* **59**: 1095-1108.

Fahl K, Stein R. 2012. Modern seasonal variability and deglacial/Holocene change of central Arctic Ocean sea ice cover: New insights from biomarker proxy records. *Earth Planetary Science Letters* **351-352**: 123-133.

Fairbanks RG. 1989. A 17 000-year glacia-eustatic sea level record: Influence of glacial melting rates on the Younger Dryas event and deep-ocean circulation. *Nature* **342**: 637-642.

Farmer EJ, Chapman MR, Andrews JE. 2008. Centennial-scale Holocene North Atlantic surface temperatures from Mg/Ca ratios in Globigerina bulloides. *Geochemistry, Geophysics, Geosystems* **9**: Q12029.

Forcino FL. 2012. Multivariate assessment of the required sample size for community paleoecological research. *Palaeogeography, Palaeoclimatology, Palaeoecology* **315-316**: 134-141.

Gammelsrød T, Leikvin Ø, Lien V, Budgell WP, Loeng H, Maslowski W. 2009. Mass and heat transports in the NE Barents Sea: Observations and models. *Journal of Marine Systems* **75**: 56-69.

Hald M, Andersson C, Ebbesen H, Jansen E, Klitegaard-Kristensen D, Risebrobakken B, Salomonsen GR, Sejrup HP, Sarnthein M, Telford R. 2007. Variations in temperature and extent of Atlantic water in the northern North Atlantic during the Holocene. *Quaternary Science Reviews* **26**: 3423-3440.

Hebbeln D, Henrich R, Baumann KH. 1998. Paleoceanography of the last glacial/interglacial cycle in the Polar North Atlantic. *Quaternary Science Reviews* **17**: 125-153.

Henrich R, Baumann KH, Huber R, Meggers H. 2002. Carbonate preservation records of the past 3 Myr in the Norwegian-Greenland Sea and the northern North Atlantic: Implications for the history of NADW production. *Marine Geology* **184**: 17-39.

Hopkins TS. 1991. The GIN Sea: A synthesis of its physical oceanography and literature review, 1972–1985. *Earth-Science Reviews* **30**: 175-318.

Ivanov VV, Alexeev VA, Repina I, Koldunov NV, Smirnov A. 2012. Tracing Atlantic water signature in the Arctic Sea ice cover East of Svalbard. *Advances in Meteorology* **2012**: 201818, 11.

Jakobsson M, Grantz A, Kristoffersen Y, Macnab R. 2004. Physiography and bathymetry of the Arctic Ocean. In *The Organic Carbon Cycle in the Arctic Ocean,* Stein R, Macdonald RW (eds). Springer: New York; 1-5.

Jernas P, Klitgaard Kristensen D, Husum K, Wilson L, Koç N. 2013. Palaeoenvironmental changes of the last two millennia on the western and northern Svalbard shelf. *Boreas* **42**: 236-255.

Johannessen T, Jansen E, Flatøy A, Ravelo AC. 1994. The relationship between surface water masses, oceanographic fronts and plaeoclimatic proxies in surface sediments of the Greenland, Iceland, Norwegian Seas. In *Carbon Cycling in the Glacial Ocean: Constraints of the Ocean's Role in Global Change*, Zahn R, Pedersen TF, Kaminski MA, Labeyrie L (eds). Springer: Berlin, 61-86.

Jonkers L, Brummer G-JA, Peeters FJC, van Aken HM, De Jong MF. 2010. Seasonal stratification, shell flux, and oxygen isotope dynamics of left-coiling N. pachyderma and T. quinqueloba in the western sub polar North Atlantic. *Paleoceanography* **25**: PA2204.

Katz ME, Cramer BS, Franzese A, Hönisch B, Miller KG, Rosenthal Y, Wright J. 2010. Traditional and emerging geochemical proxies in foraminifera. *Journal of Foraminiferal research* **40(2)**:165-192.

Kaufman D, Ager TA, Anderson NJ, Anderson PM, Andrews JT, Bartlein PJ, Brubakker LB, Coats LL, Cwynar LC, Duvall ML, Dyke AS, Edwards ME, Eisner WR, Gajewski K, Geirsdottir A, Hu FS, Jennings AE, Kaplan MR, Kerwin MW, Loshkin AV, MacDonald GM, Miller GH, Mock CJ, Oswald WW, Otto-Bliesner BL, Porinchu DF, Rühland K, Smol JP, Steig EJ, Wolfe BB. 2004. Holocene thermal maximum in the western Arctic (0 - 180 °N). *Quaternary Science Reviews* **23:** 529-560.

Kaufman DS, Schneider DP, McKay NP, Ammann CM, Bradley RS, Briffa KR, Miller GH, Otto-Bliesner BL, Overpeck JT, Vinther BM. 2009. Recent warming reverses long-term arctic cooling. *Science* **325(5945)**: 1236-1239.

Keigwin LD, Boyle EA. 1989. Late Quaternary paleochemistry of high-latitude surface waters. *Palaeogeography, Palaeoclimatology, Palaeoecology* **73**: 85-106.

Klitgaard Kristensen D, Rasmussen TL, Koç N. 2013. Paleoceanographic changes in the northern Barents Sea during the last 16 000 years – new constraints on the last deglaciation of the Svalbard-Barents Ice Sheet. *Boreas* **42**: 798-813.

Knies J, Cabedo-Sanz P, Bel, ST, Baranwal S, Fietz S, Rosell-Melé A. 2014. The emergence of modern sea ice cover in the Arctic Ocean. *Nature Communications* **5**: 5608.

Knudsen KL. 1998. Foraminiferer i Kvartær stratigrafi: Laboratorie og fremstillingsteknik samt udvalgte eksempler. *Geologisk Tidsskrift* **3**: 1-25.

Koç N, Jansen E, Haflidason H. 1993. Paleoceanographic reconstructions of surface ocean conditions in the Greenland, Iceland and Norwegian seas through the last 14 ka based on diatoms. *Quaternary Science Reviews* **12**: 115-140

Kohfeld KE, Fairbanks RG, Smith SL. 1996. *Neogloboquadrina pachyderma* (sinistral coiling) as paleoceanographic tracers in polar oceans: Evidence from northeast water polynya plankton tows, sediments traps, and surface sediments. *Paleoceanography* **11**: 679-699.

Kwok R. 2009. Outflow of Arctic Ocean sea ice into the Greenland and Barents Seas: 1979-2007. *Journal of Climate* **22(9)**: 2438-2457.

Kwok R, Maslowski W, Laxon S. 2005. On large outflows of Arctic sea-ice into the Barents Sea. *Geophysical Research Letters* **32**: L22503.

Laskar J, Robutel P, Joutel F, Gastineau M, Correia ACM, Levrard B. 2004. A long-term numerical solution for the insolation quantities of the Earth. *Astronomy and Astrophysics* **428**: 261-285.

Loeng H. 1991. Features of the physical oceanographic conditions of the Barents Sea. *Polar Research* **10**: 5-18.

Loeng H, Ozhigin V, Ådlandsvik B, Sagen H. 1993. *Current Measurements in the northeastern Barents Sea*, International Council for the Exploration of the Sea, Council Meeting 1993/C:41, Hydrographic Committee; 22.

Lubinski DJ, Polyak L, Forman SL. 2001. Freshwater and Atlantic water inflows to the deep northern Barents and Kara seas since ca 13 ^{14}Cka: foraminifera and stable isotopes. *Quaternary Science Reviews* **20**: 1851-1879.

Mangerud J, Bondevik S, Gulliksen S, Hufthammer AK, Høisæter T. 2006. Marine ^{14}C reservoir ages for 19th century whales and molluscs from the North Atlantic. *Quaternary Science Reviews* **25**: 3228-3245.

Manley TO. 1995. Branching of Atlantic Water within the Greenland-Spitsbergen Passage: An estimate of recirculation. *Journal of Geophysical Research* **100**: 20627-20634.

Massé G, Rowland SJ, Sicre M-A, Jacob J, Jansen E, Belt ST. 2008. Abrupt climate changes for Iceland during the last millennium: Evidence from high resolution sea ice reconstructions. *Earth and Planetary Science Letters* **269**: 565-569.

Méheust M, Fahl K, Stein R. 2013. Variability in modern sea surface temperature, sea ice and terrigenous input in the sub-polar North Pacific and Bering Sea: Reconstruction from biomarker data. *Organic Geochemistry* **57**: 54-64.

Méheust M, Stein R, Fahl K, Max L, Riethdorf J-R. 2015. High-resolution IP_{25}-based reconstruction of sea ice variability in the western North Pacific and Bering Sea during the past 18,000 years. *GeoMarine Letters* **36**: 101-111.

Midttun L. 1985. Formation of dense bottom water in the Barents Sea. *Deep-Sea Research* **32**: 1233-1241.

Müller J, Massé G, Stein R, Belt ST. 2009. Variability of sea ice conditions in the Fram Strait over the past 30000 years. *Nature Geoscience* **2(11**: 772-776.

Müller J, Wagner A, Fahl K, Stein R, Prange M, Lohman G. 2011. Towards quantitative sea ice reconstructions in the northern North Atlantic: A combined biomarker and numerical modelling approach. *Earth and Planetary Science Letters* **306**: 137-148.

Müller J, Werner K, Stein R, Fahl K, Moros M, Jansen E. 2012. Holocene cooling culminates in sea ice oscillations in Fram Strait. *Quaternary Science Reviews* **47**: 1-14.

Müller J, Stein R. 2014. High-resolution record of late glacial sea ice changes in Fram Strait corroborates ice-ocean interactions during abrupt climate shifts. *Earth and Planetary Science Letters* **403**: 446-455.

National Snow and Ice Data Center (NSIDC), Boulder Colorado, www.nsidc.com

Navarro-Rodriguez A, Belt ST, Knies J, Brown TA. 2013. Mapping recent sea ice conditions in the Barents Sea using the proxy biomarker IP_{25}: Implications for palaeo sea ice reconstructions. *Quaternary Science Reviews* **79**: 26-39.

Novitskiy VP. 1961. Permanent currents of the northern Barents Sea. *Trudy Gosudarstvennogo Okeanograficheskogo Instituta* **64**: 1-32. (English Translation).

Oppo DW, Fairbanks RG. 1989. Carbon isotope composition of tropical surface water during the past 22,000 years. *Paleoceanography* **4**: 333-351.

Pados T, Spielhagen RF. 2014. Species distribution and depth habitat of recent planktic foraminifera in Fram Strait, Arctic Ocean. *Polar Research* **33**: 22483.

Pfirman SL, Bauch D, Gammelsrød T. 1994. The Northern Barents Sea: water mass distribution and modification. In *The Polar Oceans and Their Role in Shaping the Global Environment*, Johannessen OM, Muench RD, Overland JE (eds). *AGU Geoph. Monog. Series.*, **85**: 77-94.

Pfuhl HA, Shackleton NJ. 2004. Two proximal, high-resolution records of foraminiferal fragmentation and their implications for changes in dissolution. *Deep-Sea Research Pt. I* **51**: 809-832.

Polyak L, Belt ST, Cabedo-Sanz P, Yamamoto M, Park YH. 2016. Holocene sea-ice conditions and circulation at the Chukchi-Alaskan margin, Arctic Ocean, inferred from biomarker proxies. *The Holocene* **26**: 1810-1821.

Rasmussen TL, Thomsen E, Slubowska MA, Jessen S, Solheim A, Koç N. 2007. Paleoceanographic evolution of the SW Svalbard margin (76 °N) since 20 000 ^{14}C yr BP. *Quaternary Research* **67**: 100-114.

Reimer PJ, Baillie MGL, Bard E, Bayliss A, Beck JW, Blackwell PG, Ramsey CB, Buck CE, Burr GS, Edwards RL, Friedrich HM, Grootes PM, Guilderson TP, Hajdas I, Heaton TJ, Hogg AG, Hughen KA, Kaiser KF, Kromer B, Mccormac FG, Manning SW, Reimer RW, Richards DA, Southon JR, Talamo S, Turney CSM, Van Der Plicht J, Weyhenmeyer CE. 2009. IntCal09 and Marine09 radiocarbon age calibration curves, 0-50 000 years cal BP. *Radiocarbon* **51**: 1111-1150.

Renssen H, Goosse H, Muscheler R. 2006. Coupled climate model simulation of Holocene cooling events: oceanic feedback amplifies solar forcing. *Climate of the Past* **2**: 79-90.

Risebrobakken B, Morros M, Ivanova EV, Chistyakova N, Rosenberg R. 2010. Climate and oceanographic variability in the SW Barents Sea during the Holocene. *The Holocene* **20**: 609-621.

Risebrobakken B, Dokken T, Smedsrud LH, Andersson C, Jansen E, Moros M, Ivanova EV. 2011. Early Holocene temperature variability in the Nordic Seas: The role of oceanic heat advection versus changes in orbital forcing. *Paleoceanography* **26**: PA4206.

Rudels B. 1987. On the mass balance of the Polar Ocean, with special emphasis on the Fram Strait. *Norsk Polarinstitutt Skrifter* **188**: 53.

Rudels B, Korhonen M, Schauer U, Pisarev S, Rabe B, Wisotzki A. 2014. Circulation and transformation of Atlantic water in the Eurasian Basin and the contribution of the Fram Strait inflow branch to the Arctic Ocean heat budget. *Progress in Oceanography* **132**: 128-152.

Sakshaug E, Bjørge A, Gulliksen B, Loeng H, Mehlum F. 1992. *Økosystem Barentshavet*. Norges Allmenvitenskapelige Forskningsråd, Norges Fiskeriforskningsråd, Miljøverndepartementet, 304.

Sarnthein M, Van Kreveld S, Erlenkeuser H, Grootes PM, Kucera M, Pflaumann U, Schulz M. 2003. Centennial-to-millennial-scale periodicities of Holocene climate and sediment injections off the western Barents shelf, 75 °N. *Boreas* **32**: 447-461.

Schauer U, Loeng H, Rudels B, Ozhigin VK, Dieck W. 2002. Atlantic Water flow through the Barents and Kara Seas. *Deep-Sea Research Pt. I* **49**: 2281-2298.

Screen JA, Simmonds I. 2010. The central role of diminishing sea ice in recent Arctic temperature amplification. *Nature* **464**: 1334-1337.

Serreze MC, Francis JA. 2006. The arctic amplification debate. *Climate Change* **76(3-4)**: 241-264.

Serreze M, Barrett A, Slater A, Steele M, Zhang J, Tenberth K. 2007. The large-scale energy budget of the Arctic. *Journal of Geophysical Research* **112**: D11122.

Shimada K, Kamoshida T, Itoh M, Nishino S, Carmack E, McLaughlin F, Zimmermann S, Proshutinsky A. 2006. Pacific Ocean inflow: Influence on catastrophic reduction of sea ice cover in the Arctic Ocean. *Geophysical Research Letters* **33**: L08605

Simstich J, Sarnthein M, Erlenkeuser H. 2003. Paired $\delta^{18}O$ signals of N. pachyderma (s) and T. quinqueloba show thermal stratification structure in the Nordic Seas. *Marine Micropaleontology* **48**: 107-125.

Skirbekk K, Klitgaard Kristensen D, Rasmussen TL, Koç N, Forwick M. 2010. Holocene climate variations at the entrance to a warm Arctic fjord: evidence from Kongsfjorden trough, Svalbard. *Geological society, London, Special Publications 2010* **344**: 289-304.

Slubowska MA, Koç N, Rasmussen TL, Klitgaard-Kristensen D. 2005. Changes in the flow of Atlantic water into the Arctic Ocean since the last deglaciation: Evidence from the northern Svalbard continental margin, 80N. *Paleoceonography* **20**: PA4014.

Smedsrud LH, Esau I, Ingvaldsen RB, Eldevik T, Haugan PM, Li C, Lien VS, Olsen A, Omar AM, Otterå OH, Risebrobakken B, Sandø AB, Semenov VA, Sorokina SA. 2013. The role of the Barents Sea in the Arctic climate system. *Reviews of Geophysics* **51(3)**: 415-449.

Smik L, Cabedo-Sanz P, Belt ST. 2016. Semi-quantitative estimates of paleo Arctic sea ice concentration based on source-specific highly branched isoprenoid alkenes: A further development of the PIP25 index. *Organic Geochemistry* **92**: 63-69.

Smith WO, Sakshaug E. 1990. Polar phytoplankton. In *Polar oceanography, Part B: Chemistry, Biology and Geology,* Smith WO (ed). Academic Press: New York; 447-525.

Sorteberg A, Kvingedal B. 2006. Atmospheric forcing on the Barents Sea winter ice extent. *Journal of Climate* **19**: 4772-4784.

Spielhagen RF, Erlenkeuser H. 1994. Stable oxygen and carbon isotopes in planktic foraminifera from the Arctic Ocean surface sediments: Reflection of the low salinity surface water layer. *Marine Geology* **119**:227-250.

Spielhagen RF, Werner K, Aagaard-Sørensen S, Zamelczyk K, Kandiano E, Budeus G, Husum K, Marchitto T, Hald M. 2011. Enhanced modern heat transfer to the Arctic by warm Atlantic water. *Science* **331**: 450-453.

Stangeew E. 2001. *Distribution and isotopic composition of living planktonic foraminifera N. pachyderma (sinistral) and T. quinqueloba in the high latitude North Atlantic*. Ph.D. thesis, Math.-Naturwiss. Fak., Christian-Albrechts-Univ., Kiel, Germany. (Available at http://e-diss.uni-kiel.de/diss_464/pp).

Stein R, Fahl K, Schade I, Manerung A, Wassmuth S, Niessen F, Nam S. 2016a. Holocene variability in sea ice cover, primary production, and Pacific-Water inflow and climate change in the Chukchi and East Siberian Seas (Arctic Ocean). *Journal of Quaternary Science* ISSN 0267-8179, DOI:10.1002/jqs.2929.

Stein R, Fahl K, Schrekck M, Knorr G, Niessen F, Forwick M, Gebhardt C, Jensen L, Kaminski M, Kopf A, Matthiessen J, Jokat W, Lohmann G. 2016b. Evidence for ice-free summers in the late Miocene central Arctic Ocean. *Nature Communications* **7**: 11148.

Steinsund PI, Hald M. 1994. Recent carbonate dissolution in the Barents Sea: Paleoceanographic applications. *Marine Geology* **117**: 303-316.

Stroeve J, Holland MM, Meier W, Scambos T, Serreze M. 2007. Arctic sea ice decline: Faster than forecast. *Geophysical Research Letters* **34**:L09501.

Stroeve J, Serreze MC, Holland MM, Kay JE, Malanik J, Barrett AP. 2012. The Arctic's rapidly shrinking sea ice cover: a research synthesis. *Climate Change* **110**:1005-1027.

Stuiver M, Reimer PJ. 1993. Extended ^{14}C data base and revised CALIB 3.0 ^{14}C age calibration program. *Radiocarbon* **35**: 215-230.

Vare LL, Massé G, Gregory TR, Smart CW, Belt ST. 2009. Sea ice variations in the central Canadian Arctic Archipelago during the Holocene. *Quaternary Science Reviews* **28**: 1354-1366.

Vare LL, Massé G, Belt ST. 2010. A biomarker-based reconstruction of sea ice conditions for the Barents Sea in recent centuries. *The Holocene* **20(4)**: 637-643.

Vinje TE. 1977. Sea ice conditions in the European sector of the marginal seas of the Arctic, 1966-75. *Aarbok Norsk Polarinstitutt* **1975**: 163-174.

Vinje T. 2001. Anomalies and trends of sea ice extent and atmospheric circulation in the Nordic Seas during the period 1864-1998. *Journal of Climate* **14(3)**: 255-267.

Volkmann R. 2000. Planktic foraminifers in the outer Laptev Sea and the Fram Strait: Modern distribution and ecology. *Journal Foraminiferal Research* **30**: 157-176.

Wassmann P, Reigstad M, Haug T, Rudels B, Carroll ML, Hop H, Gabrielsen GW, Falk-Petersen S, Denisenko SG, Arashkevich E, Slagstad D, Pavlova O. 2006. Food webs and carbon flux in the Barents Sea. *Progress in Oceanography* **71**: 232-287.

Wassmann P. 2011. Arctic marine ecosystems in an era of rapid climate change. *Progress in Oceanography* **90**: 1-17.

Weckström K, Massé G, Collins LG, Hanhijärvi S, Bouloubassi I, Sicre M-A, Seidenkrantz M-S, Schmidt S, Andersen TJ, Andersen ML, Hill B, Kuijpers A. 2013. Evaluation of the sea ice proxy IP_{25} against observational and diatom proxy data in the SW Labrador Sea. *Quaternary Science Reviews* **79**: 53-62.

Werner K, Spielhagen RF, Bauch D, Hass HC, Kandiano E. 2013. Atlantic Water advection versus sea ice advances in the eastern Fram Strait during the last 9 ka: Multi proxy evidence for a two-phase Holocene. *Paleoceanography* **28**: 283-295.

Werner K, Frank M, Teschner C, Müller J, Spielhagen RF. 2014. Neoglacial change in deep water exchange and increase of sea ice transport through eastern Fram Strait: evidence from radiogenic isotopes. *Quaternary Science Reviews* **92**: 190-207.

Wilson LJ, Hald M, Godtliebsen F. 2011. Foraminiferal faunal evidence of twentieth-century Barents Sea warming. *The Holocene* **21(4)**: 527-537.

Woodgate RA, Weingartner TJ, Lindsay R. 2010. The 2007 Bering Strait oceanic heat flux and anomalous Arctic sea-ice retreat. *Geophysical Research Letters* **37**: L01602.

Xiao X, Fahl K, Stein R, 2013. Biomarker distributions in surface sediments from the Kara and Laptev seas (Arctic Ocean): indicators for organic-carbon sources and sea ice coverage. *Quaternary Science Reviews* **79**: 40-52.

Xiao X, Fahl K, Müller J, Stein R. 2015a. Sea ice distribution in the modern Arctic Ocean: Biomarker records from trans-Arctic Ocean surface sediments. *Geochimica Cosmochimica Acta* **155**: 16-29.

Xiao X, Stein R, Fahl K. 2015b. MIS 3 to MIS 1 temporal and LGM spatial variability in Arctic Ocean sea ice cover: Reconstruction from biomarkers. *Paleoceanography* **30**: 969-983.

Yang S, Christensen JH. 2012. Arctic sea ice reduction and European cold winters in CMIP5 climate change experiments. *Geophysical Research Letters* **39**: L20707.

Zamelczyk K, Rasmussen TL, Husum K, Haflidason H, de Vernal A, Krogh Ravna E, Hald M, Hillaire-Marcel C. 2012. Paleoceanographic changes and calcium carbonate dissolution in the central Fram Strait during the last 20 ka yr. *Quaternary Research* **78**: 405-416

Zamelczyk K, Rasmussen TL, Husum K, Hald M. 2013. Marine calcium carbonate preservation vs. climate change over the last two millennia in the Fram Strait: Implications for planktic foraminiferal paleostudies. *Marine Micropaleontology* **98**: 14-27.

Årthun M, Eldevik T, Smedsrud LH, Skagseth Ø, Ingvaldsen R. 2012. Quantifying the influence of Atlantic heat on Barents Sea ice variability and retreat. *Journal of Climate* **25**: 4736-4743.

Figure captions

Table 1. Depth-age model of NP05-11-70GC calibrated using Calib 6.1.1 (Stuiver and Reimer, 1993), the Marine09 calibration curve (Reimer *et al*., 2009) and a local reservoir age (ΔR) of 105±24 after Mangerud *et al*. (2006).

Figure 1. The modern oceanography is presented on a bathymetric map of the Barents Sea area. The core location of NP05-11-70GC is indicated by a black star, whereas previously published records are indicated by number: (1) Risebrobakken *et al*. (2010), (2) Wilson *et al*. (2011), (3) Berben *et al*. (2014), (4) Rasmussen *et al*. (2007), (5) Müller *et al*. (2012); Werner *et al*. (2013), (6) Skirbekk *et al*. (2010); Jernas *et al*. (2013), (7) Müller *et al*. (2009), (8) Slubowska *et al*. (2005); Jernas *et al*. (2013), (9) Klitgaard Kristensen *et al*. (2013), (10) Lubinski *et al*. (2001), (11) Duplessy *et al*. (2001); (2005), (12) Risebrobakken *et al*. (2011), and (13) Duplessy *et al*. (2005). Northern Barents Sea Opening (NBSO), Barents Sea Opening (BSO), Barents Sea Exit (BSX). (a) The main surface currents (Hopkins, 1991). Atlantic Water (red): Norwegian Atlantic Current (NwAC), North Cape Current (NCaC), West Spitsbergen Current (WSC), Return Atlantic Current (RAC), Yermak Branch (YB) and Svalbard Branch (SB). Polar Water (blue): Bear Island Current (BIC) and East Spitsbergen Current (ESC). Coastal Water (black). (b) Seasonal sea ice margins (April (purple) and August (orange)) for the period 1981–2010 (National Snow and Ice Data Centre (NSIDC) Boulder Colorado, www.nsidc.com). The observed sea ice margin for April (dotted) and August (dashed) from historical data for four sub-periods between 1870 and 2002: 1870–1920 (red), 1921–1961 (yellow), 1962–1988 (pink) and 1989–2002 (black) (Divine and Dick, 2006). (c) Temperature (black) and Salinity (grey) profile at the NP05-11-70GC core site (78.40° N, 32.42° E). Water masses are defined according Gammelsrød *et al*. (2009).

Figure 2. Depth-age model of NP05-11-70GC. Calibrated radiocarbon ages versus depth with a linear interpolation between the dated levels. Error bars indicate the sampled depth intervals and a 2-σ error on the calibrated ages.

Figure 3. Biomarker analysis versus cal a BP and core depth. The black diamonds on the Y-axis denote the AMS ^{14}C converted to calibrated radiocarbon ages. (a) Sea ice biomarker IP_{25} versus age. (b) Phytoplankton biomarker brassicasterol versus age. (c) Phytoplankton-derived HBI III biomarker versus age. Biomarker concentrations are normalized to total organic carbon (black) and to sediment mass (grey). (d) Total organic carbon versus age. (e) P_BIP_{25} versus age. (f) $P_{III}IP_{25}$ versus age. >5% summer sea ice concentration (SuSIC) is also indicated when $P_{III}IP_{25}$ exceeds a value of 0.8 (Smik *et al*., 2016). (g) Estimated spring sea ice concentration (SpSIC) versus age.

Figure 4. Planktic foraminiferal fauna and preservation indicator analysis versus cal a BP and core depth. The black diamonds on the Y-axis denote the AMS ^{14}C converted to calibrated radiocarbon ages. (a) Total planktic foraminiferal concentration versus age. (b) Planktic foraminiferal fragmentation versus age. (c) Mean shell weight of *N. pachyderma* versus age. (d-i) Species-specific relative abundance versus age.

Figure 5. Stable isotopes analysis performed on *N. pachyderma* versus cal a BP and core depth. The black diamonds on the X-axis denote the AMS ^{14}C converted to calibrated radiocarbon ages. (a) $\delta^{18}O$ measurements corrected for ice volume effect after Fairbanks (1989) (black) and uncorrected $\delta^{18}O$ measurements (grey) versus age. (b) $\delta^{13}C$ measurements versus age.

Figure 6. Multi-proxy analysis versus cal a BP and core depth. The black diamonds on the Y-axis denote the AMS ^{14}C converted to calibrated radiocarbon ages. (a) July insolation at 78° N (Laskar *et al*., 2004) (note the reversed axis) versus age. (b) Sea ice biomarker IP_{25} versus age. Concentrations are normalized to total organic carbon (black line) and to sediment mass (grey line). (c) $P_{III}IP_{25}$ versus age. >5% summer sea ice concentration (SuSIC) is also indicated when $P_{III}IP_{25}$ exceeds a value of 0.8 (Smik *et al., 2016).* (d) Estimated spring sea ice concentration (SpSIC) versus age. (e) $\delta^{18}O$ measurements corrected for ice volume effect after Fairbanks (1989) versus age. (f) Relative abundance of *N. pachyderma* versus age. (g) Planktic foraminiferal concentration versus age. (b-d) The in dark grey highlighted period reflects decreased sea ice conditions, whereas the in light grey highlighted periods indicate increased sea ice conditions. (e-g) The in grey highlighted periods are characterized by an increased influence of Atlantic Water.

Figure 7. Illustrations of the proposed seasonal sea ice scenarios at the NP05-11-70GC core location (black star). The shaded areas surrounding the dotted lines represent the proposed variability of the sea ice margin for March (black), April (purple) and August (orange), whereas the numbers indicate the core locations of previous studies: (1) Berben *et al*. (2014), (2) Müller *et al*. (2012), (3) Müller *et al*. (2009), (4) Klitgaard Kristensen *et al*. (2013), and (5) Duplessy *et al*. (2001). (a) Period I. (b) Period II. (c) Period III (dotted lines with shaded areas) and present day situation (full lines) based on mean sea ice margins (1981–2010) (National Snow and Ice Data Centre (NSIDC) Boulder Colorado, www.nsidc.com).

Table 1

Lab ID	Core depth (cm)	Material	Uncorrected AMS ^{14}C age	1σ	Calibrated age 2-σ range	Calibrated age used in depth-age model (cal a BP)
Beta-331327	37 - 43	Benthic foraminifera	2780	30	2281–2496	2389
Beta-346803	67 - 72	Benthic foraminifera	6110	40	6298–6536	6417
Beta-331328	122 - 127	Benthic foraminifera	8870	50	9307–9527	9417
Beta-331329	213 - 230	Benthic foraminifera	> 43500			

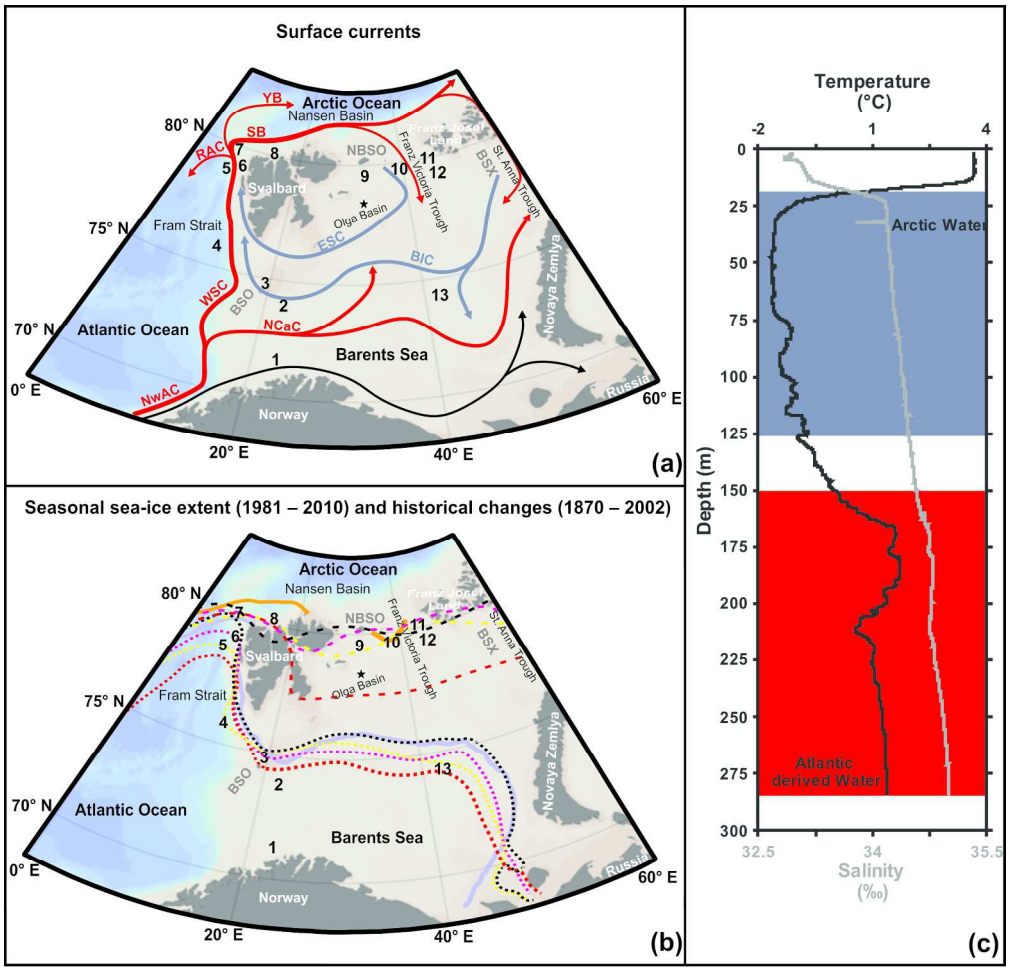

Figure 1. The modern oceanography is presented on a bathymetric map of the Barents Sea area. The core location of NP05-11-70GC is indicated by a black star, whereas previously published records are indicated by number: (1) Risebrobakken et al. (2010), (2) Wilson et al. (2011), (3) Berben et al. (2014), (4) Rasmussen et al. (2007), (5) Müller et al. (2012); Werner et al. (2013), (6) Skirbekk et al. (2010); Jernas et al. (2013), (7) Müller et al. (2009), (8) Slubowska et al. (2005); Jernas et al. (2013), (9) Klitgaard Kristensen et al. (2013), (10) Lubinski et al. (2001), (11) Duplessy et al. (2001); (2005), (12) Risebrobakken et al. (2011), and (13) Duplessy et al. (2005). Northern Barents Sea Opening (NBSO), Barents Sea Opening (BSO), Barents Sea Exit (BSX). (a) The main surface currents (Hopkins, 1991). Atlantic Water (red): Norwegian Atlantic Current (NwAC), North Cape Current (NCaC), West Spitsbergen Current (WSC), Return Atlantic Current (RAC), Yermak Branch (YB) and Svalbard Branch (SB). Polar Water (blue): Bear Island Current (BIC) and East Spitsbergen Current (ESC). Coastal Water (black). (b) Seasonal sea ice margins (April (purple) and August (orange)) for the period 1981–2010 (National Snow and Ice Data Centre (NSIDC) Boulder Colorado, www.nsidc.com). The observed sea ice margin for April (dotted) and August (dashed) from historical data for four sub-periods between 1870 and 2002: 1870–1920 (red), 1921–1961 (yellow), 1962–1988 (pink) and 1989–2002 (black) (Divine and Dick, 2006). (c) Temperature (black) and Salinity (grey) profile at the NP05-11-70GC core site (78.40° N, 32.42° E). Water masses are defined according Gammelsrød et al. (2009).

210x202mm (300 x 300 DPI)

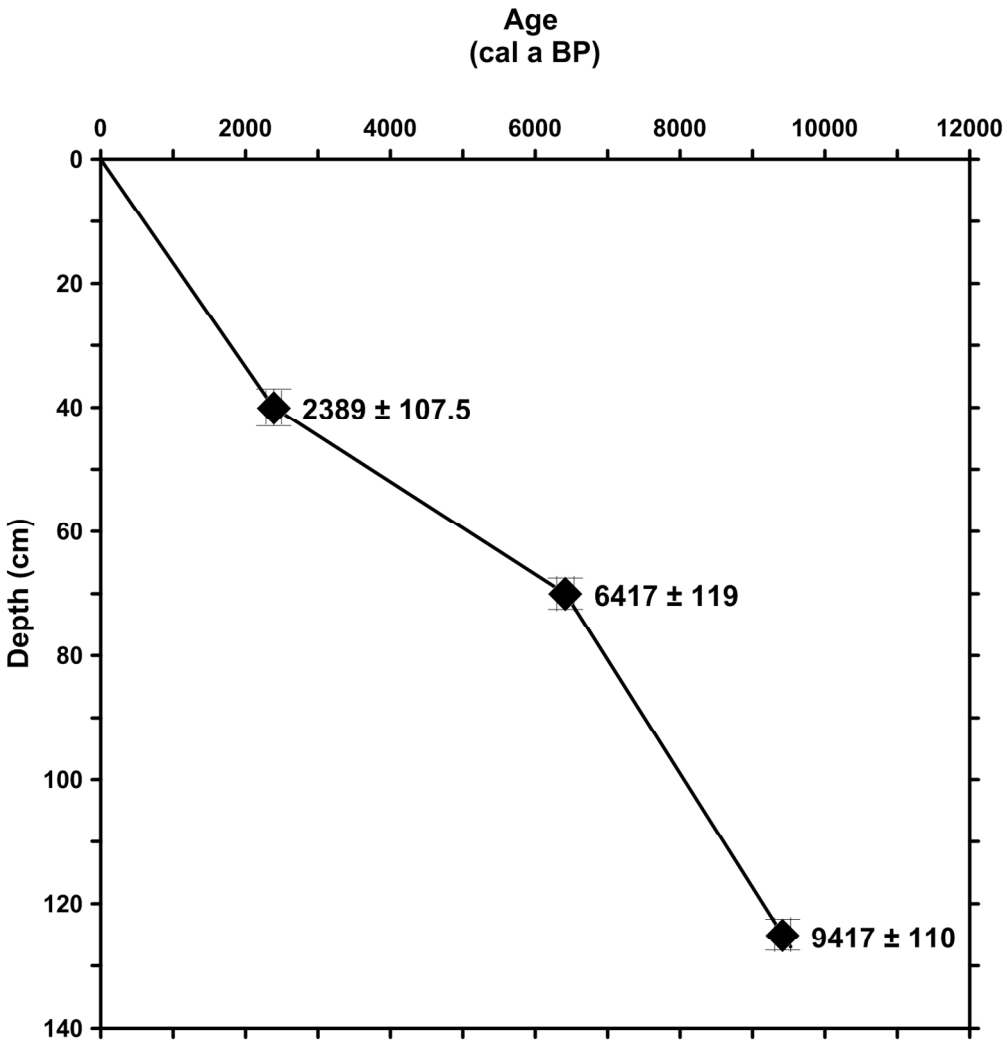

Figure 2. Depth-age model of NP05-11-70GC. Calibrated radiocarbon ages versus depth with a linear interpolation between the dated levels. Error bars indicate the sampled depth intervals and a 2-σ error on the calibrated ages.

146x151mm (300 x 300 DPI)

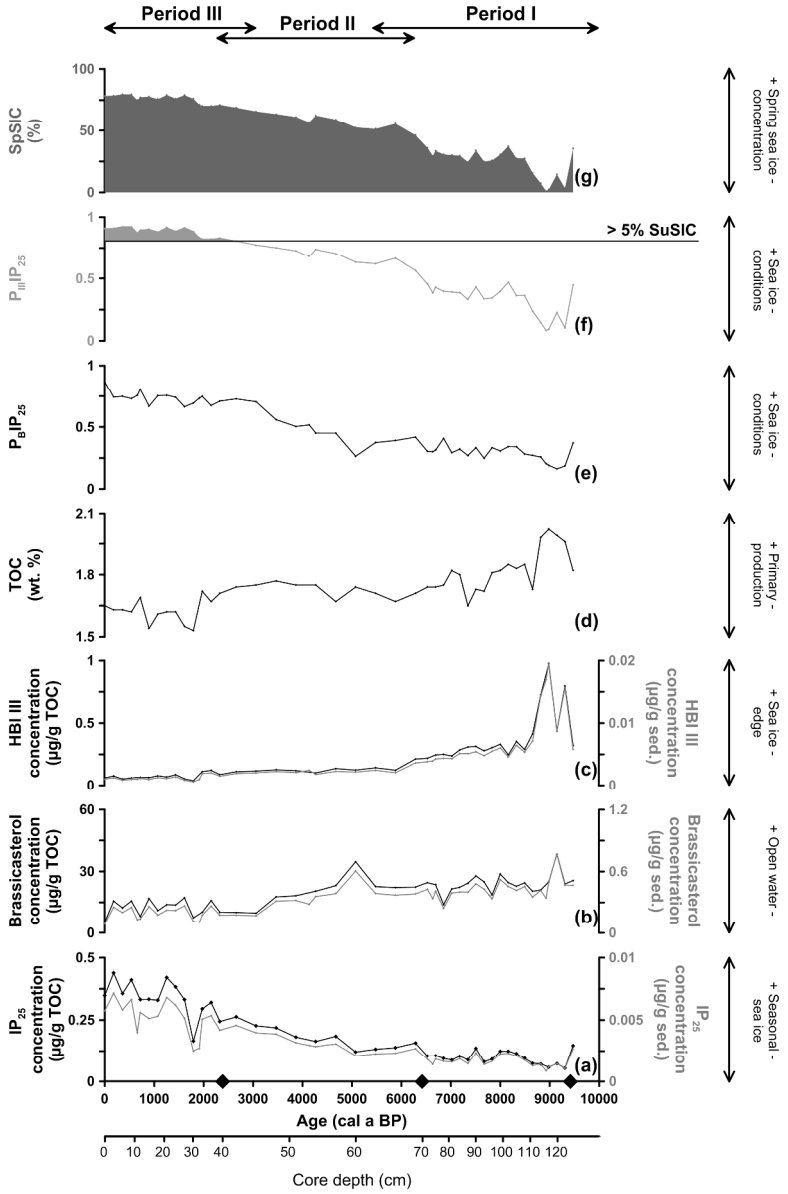

Figure 3. Biomarker analysis versus cal a BP and core depth. The black diamonds on the Y-axis denote the AMS 14C converted to calibrated radiocarbon ages. (a) Sea ice biomarker IP25 versus age. (b) Phytoplankton biomarker brassicasterol versus age. (c) Phytoplankton-derived HBI III biomarker versus age. Biomarker concentrations are normalized to total organic carbon (black) and to sediment mass (grey). (d) Total organic carbon versus age. (e) PBIP25 versus age. (f) PIIIIP25 versus age. >5% summer sea ice concentration (SuSIC) is also indicated when PIIIIP25 exceeds a value of 0.8 (Smik et al., 2016). (g) Estimated spring sea ice concentration (SpSIC) versus age.

199x308mm (300 x 300 DPI)

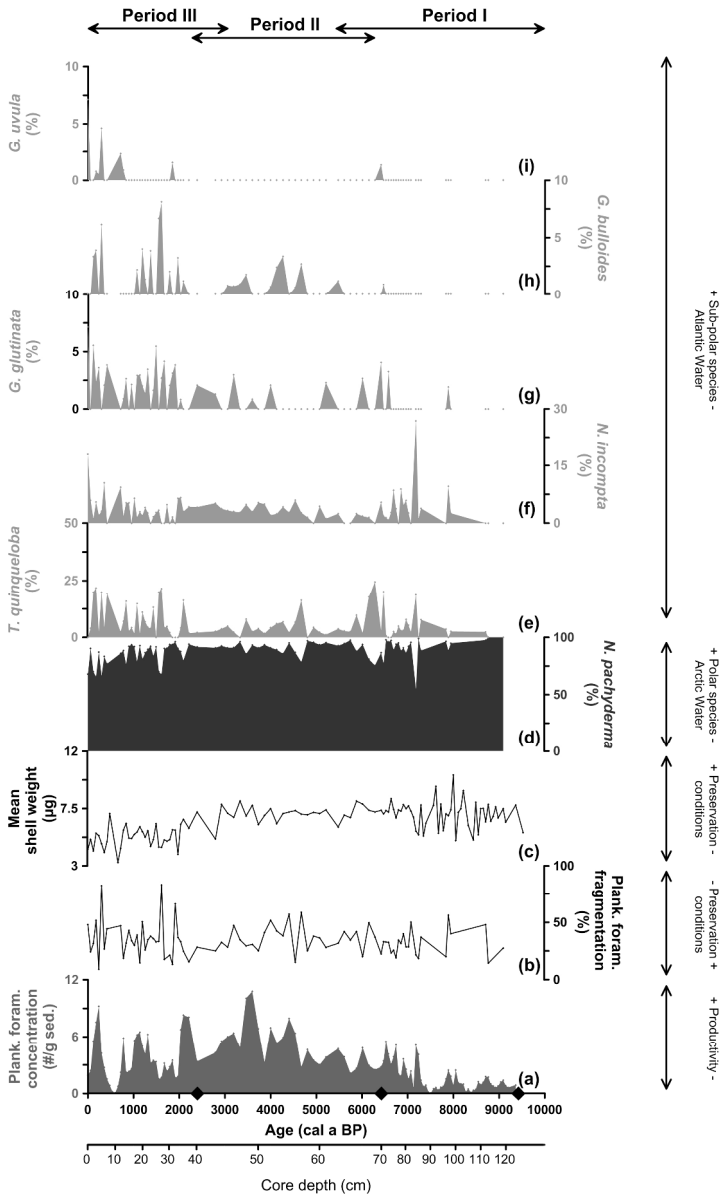

Figure 4. Planktic foraminiferal fauna and preservation indicator analysis versus cal a BP and core depth. The black diamonds on the Y-axis denote the AMS 14C converted to calibrated radiocarbon ages. (a) Total planktic foraminiferal concentration versus age. (b) Planktic foraminiferal fragmentation versus age. (c) Mean shell weight of N. pachyderma versus age. (d-i) Species-specific relative abundance versus age.

198x334mm (300 x 300 DPI)

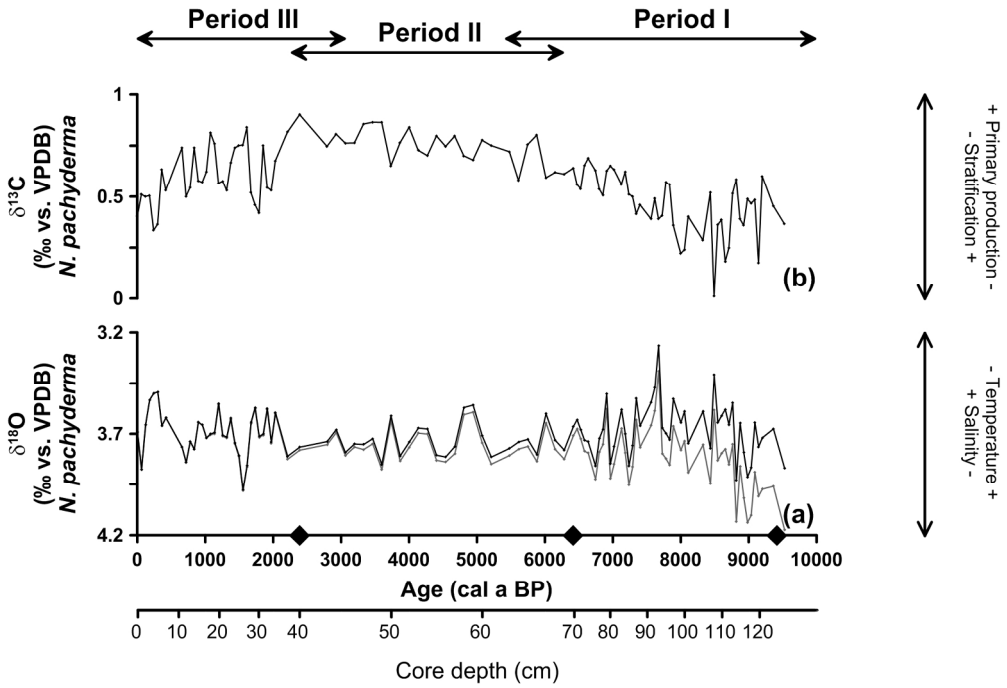

Figure 5. Stable isotopes analysis performed on N. pachyderma versus cal a BP and core depth. The black diamonds on the X-axis denote the AMS 14C converted to calibrated radiocarbon ages. (a) δ18O measurements corrected for ice volume effect after Fairbanks (1989) (black) and uncorrected δ18O measurements (grey) versus age. (b) δ13C measurements versus age.

187x130mm (300 x 300 DPI)

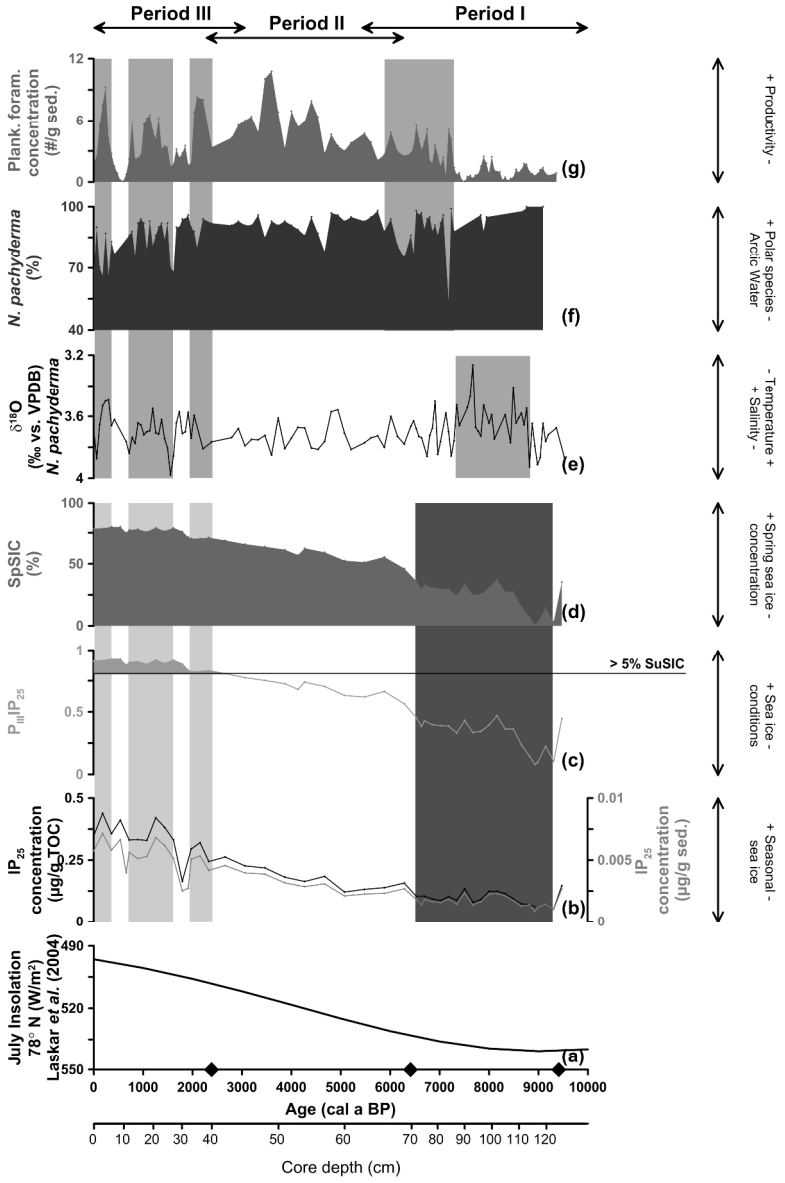

Figure 6. Multi-proxy analysis versus cal a BP and core depth. The black diamonds on the Y-axis denote the AMS 14C converted to calibrated radiocarbon ages. (a) July insolation at 78° N (Laskar et al., 2004) (note the reversed axis) versus age. (b) Sea ice biomarker IP25 versus age. Concentrations are normalized to total organic carbon (black line) and to sediment mass (grey line). (c) PIIIIP25 versus age. >5% summer sea ice concentration (SuSIC) is also indicated when PIIIIP25 exceeds a value of 0.8 (Smik et al., 2016). (d) Estimated spring sea ice concentration (SpSIC) versus age. (e) δ18O measurements corrected for ice volume effect after Fairbanks (1989) versus age. (f) Relative abundance of N. pachyderma versus age. (g) Planktic foraminiferal concentration versus age. (b-d) The in dark grey highlighted period reflects decreased sea ice conditions, whereas the in light grey highlighted periods indicate increased sea ice conditions. (e-g) The in grey highlighted periods are characterized by an increased influence of Atlantic Water.

198x308mm (300 x 300 DPI)

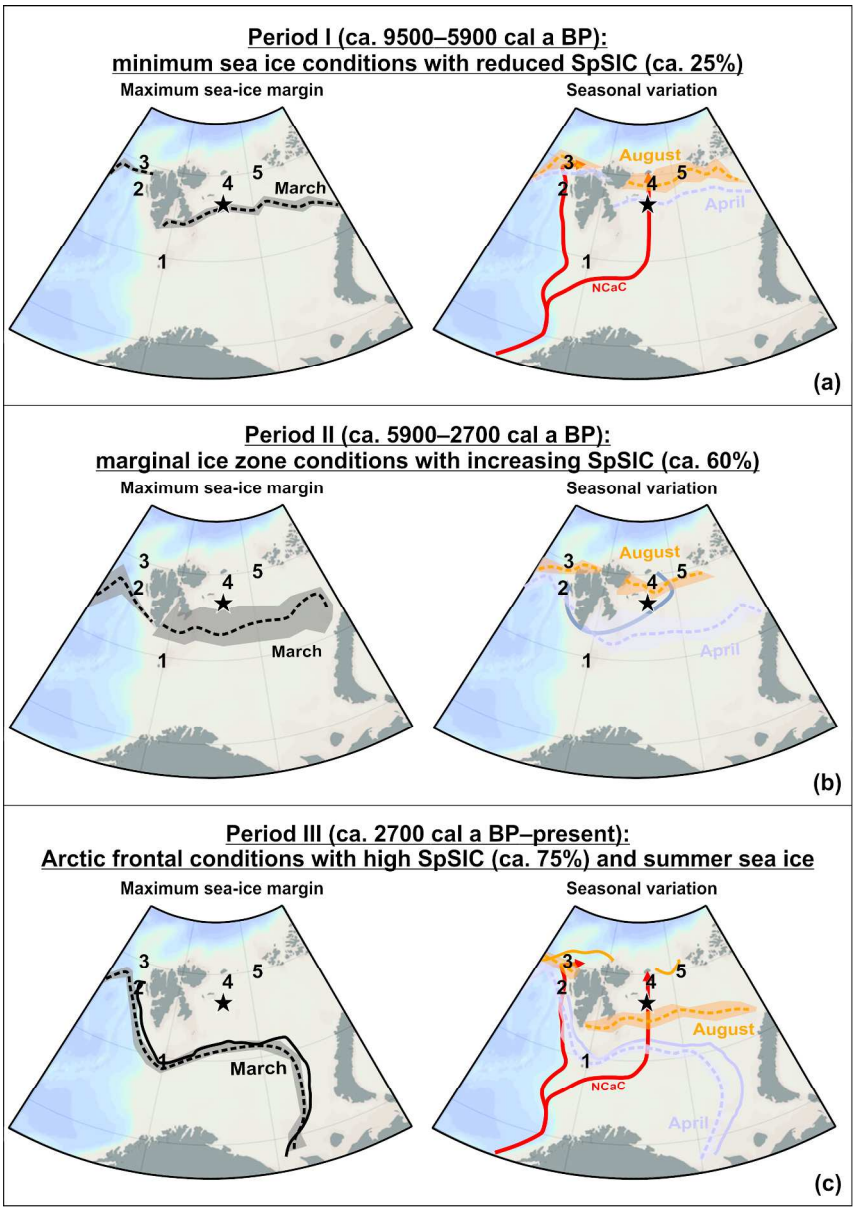

Figure 7. Illustrations of the proposed seasonal sea ice scenarios at the NP05-11-70GC core location (black star). The shaded areas surrounding the dotted lines represent the proposed variability of the sea ice margin for March (black), April (purple) and August (orange), whereas the numbers indicate the core locations of previous studies: (1) Berben et al. (2014), (2) Müller et al. (2012), (3) Müller et al. (2009), (4) Klitgaard Kristensen et al. (2013), and (5) Duplessy et al. (2001). (a) Period I. (b) Period II. (c) Period III (dotted lines with shaded areas) and present day situation (full lines) based on mean sea ice margins (1981–2010) (National Snow and Ice Data Centre (NSIDC) Boulder Colorado, www.nsidc.com).

210x296mm (300 x 300 DPI)